The dendritic cell cytoskeleton promotes T cell adhesion and activation by constraining ICAM-1 mobility

William A. Comrie, Shuixing Li, Sarah Boyle, and Janis K. Burkhardt

Department of Pathology and Laboratory Medicine, Children's Hospital of Philadelphia and Perelman School of Medicine at the University of Pennsylvania, Philadelphia, PA 19102

Integrity of the dendritic cell (DC) actin cytoskeleton is essential for T cell priming, but the underlying mechanisms are poorly understood. We show that the DC F-actin network regulates the lateral mobility of intracellular cell adhesion molecule 1 (ICAM-1), but not MHCII. ICAM-1 mobility and clustering are regulated by maturation-induced changes in the expression and activation of moesin and α-actinin-1, which associate with actin filaments and the ICAM-1 cytoplasmic domain. Constrained ICAM-1 mobility is important for DC function, as DCs expressing a high-mobility ICAM-1 mutant lacking the cytoplasmic domain exhibit diminished antigen-dependent conjugate formation and T cell priming. These defects are associated with inefficient induction of leukocyte functional antigen 1 (LFA-1) affinity maturation, which is consistent with a model in which constrained ICAM-1 mobility opposes forces on LFA-1 exerted by the T cell cytoskeleton, whereas ICAM-1 clustering enhances valency and further promotes ligand-dependent LFA-1 activation. Our results reveal an important new mechanism through which the DC cytoskeleton regulates receptor activation at the immunological synapse.

Introduction

T cell activation by antigen-presenting cells (APCs) requires the formation of a specialized cell–cell contact termed the immunological synapse (IS), which facilitates the assembly of dynamic molecular signaling complexes. The T cell acto-myosin network plays a critical role in spatio-temporal regulation of IS organization (Billadeau et al., 2007; Burkhardt et al., 2008). Importantly, this network does not function as a static scaffold; continued actin retrograde flow is required to maintain T cell signaling (Babich et al., 2012). Recently, it has been suggested that cytoskeletal flow promotes signaling by exerting force on T cell signaling molecules that are bound to ligands on the surface of the APC (Ma and Finkel, 2010; Springer and Dustin, 2012; Chen and Zhu, 2013).

Among the various activating and coactivating receptors on the surface of T cells, the T cell receptor (TCR) and the integrin leukocyte functional antigen 1 (LFA-1) have been proposed to act as mechanosensors, molecules that respond to physical force by changing conformation or initiating downstream signaling. Evidence that the TCR functions as a mechanosensor comes from conformational analysis of the TCR bound to activating antibodies, which shows that force applied tangentially to the peptide-bound major histocompatibility antigen (pMHC)/TCR bond can initiate downstream signaling (Kim et al., 2009, 2012). Moreover, multiple groups have observed that soluble monomeric pMHC is poorly suited to activating T cells, even at extremely high concentrations (Boniface et al., 1998; Hamad et al., 1998; Casares et al., 1999; Appel et al., 2000; Cochran et al., 2000), despite TCR–pMHC half-lives otherwise associated with TCR triggering in a 2D environment (Huppa et al., 2010), whereas surface-bound monomeric pMHC can trigger TCR activation in an F-actin–dependent manner (Ma et al., 2008; Xie et al., 2012). One interpretation of this finding is that forces on the TCR provided by the F-actin network, when opposed by surface-bound pMHC, produce a deformation in the TCR that induces signaling. Finally, agonist TCR–pMHC interactions have recently been found to engage in catch-bond type interactions in which force prolongs bond lifetime, and mechanically pulling on single pMHC–TCR bonds can initiate calcium signaling (Liu et al., 2014).

Mechanotransduction by the TCR remains controversial, and many details remain to be elucidated. In contrast, the role

Correspondence to Janis K. Burkhardt: jburkhar@mail.med.upenn.edu

Abbreviations used in this paper: APC, antigen-presenting cell; CFSC, carboxyfluorescein succinimidyl ester; DC, dendritic cell; ICAM-1, intracellular cell adhesion molecule 1; IMDM, Iscove's modified Dulbecco's medium; IS, immunological synapse; LFA-1, leukocyte functional antigen 1; pMHC, peptide-bound major histocompatibility antigen; TCR, T cell receptor; WT, wild type.

© 2015 Comrie et al. This article is distributed under the terms of an Attribution–Noncommercial–Share Alike–No Mirror Sites license for the first six months after the publication date (see http://www.rupress.org/terms). After six months it is available under a Creative Commons License (Attribution–Noncommercial–Share Alike 3.0 Unported license, as described at http://creativecommons.org/licenses/by-nc-sa/3.0/).

The Rockefeller University Press $30.00
J. Cell Biol. Vol. 208 No. 4 457–473
www.jcb.org/cgi/doi/10.1083/jcb.201406120

THE JOURNAL OF CELL BIOLOGY

Downloaded from http://rupress.org/jcb/article-pdf/208/4/457/1586664/jcb_201406120.pdf by guest on 08 February 2026

of force in integrin activation has been well established. Integrins are heterodimeric transmembrane proteins composed of an α and a β chain, and are the main adhesion receptors that stabilize T cell–APC contacts. In addition to acting as adhesion receptors, integrins can function as signaling molecules in a process termed "outside-in" signaling. Integrin adhesion and signaling functions occur coordinately, and together, these processes lower the threshold for T cell activation. For example, engagement of the β1 integrin very late antigen 4 (VLA-4) enhances calcium mobilization and stimulation of the NF-AT promoter (Nguyen et al., 2008). The canonical integrin involved in IS formation in naïve T cells is the β2 integrin LFA-1. Engagement of LFA-1 enhances activation of key T cell signaling components such as PI3K, PLCγ1, ERK1/2, JNK, and Src (Ni et al., 2001; Perez et al., 2003; Li et al., 2009). The adapter molecule SLP-76 also functions in outside-in integrin signaling, possibly by recruiting ADAP to sites of LFA-1 engagement (Baker et al., 2009; Wang et al., 2009). Stronger activation of early signaling events upon co-stimulation through LFA-1 has been shown to lead to enhanced IL-2 production, T cell proliferation, and production of type 1 cytokines (Perez et al., 2003; Varga et al., 2010). Finally, it is known that intracellular cell adhesion molecule 1 (ICAM-1) expression on APCs is required for the proper generation of T cell memory responses (Parameswaran et al., 2005; Scholer et al., 2008).

To tightly regulate adhesion and outside-in signaling, integrin activity is controlled through a series of conformational changes, relying on extracellular signals and ligand binding to modulate the affinity for ligand (for review see Hogg et al., 2011). Integrins exist in three major conformational states. In resting T cells, they exist in a low affinity, "closed," conformation in which the α and β chains are bent and the ligand binding I domain lies proximal to the plasma membrane. In a process is termed "inside-out signaling," external stimuli such as engagement of chemokine receptors or TCR induce the adoption of an intermediate affinity "extended" conformation in which the α and β chains are straight and the I domain is distal to the plasma membrane. This process depends in part upon association of talin and kindlins with the cytoplasmic tail of the β chain, relieving charge interactions with the α chain (Tadokoro et al., 2003; Feng et al., 2012). Finally, binding of ligand can induce the high-affinity, "extended-open" conformation in which the α and β chains are straight and their cytoplasmic domains have been separated. Importantly, integrins are known to engage in catch bonds, in which force applied to the integrin–ligand pair extends bond lifetime and assists LFA-1 maturation from the intermediate-affinity extended conformation to the high-affinity extended-open conformation (Zhu et al., 2008; Kong et al., 2009; Chen et al., 2010a). Separation of the cytoplasmic tails is thought to be facilitated by cytoskeletal forces, transmitted to the β chain via actin binding of talin and kindlins (Springer and Dustin, 2012). On the surface of T cells, transition from the intermediate- to the high-affinity form of LFA-1 is energy dependent, which is consistent with the idea that force provided by the cytoskeleton is required (Schürpf and Springer, 2011). The ability to provide a co-stimulatory, outside-in, signal is highly dependent on the physical separation of the cytoplasmic tails (Kim et al., 2003), and inhibiting tail separation prevents cell spreading and protein phosphorylation downstream of the prototypic integrin αIIbβ3 (Zhu et al., 2007).

To achieve tail separation and adoption of the extended-open conformation, pulling forces on the integrin β chain likely need to be opposed by retention forces on the integrin ligand. In support of this idea, Perez et al. (2003) showed that soluble ICAM-1 fails to co-stimulate T cell priming. In agreement with this, glass-immobilized, but not soluble, ICAM-1 triggers LFA-1 to adopt the extended-open, signaling-competent conformation (Feigelson et al., 2010). Additionally, natural killer cells respond best to target cells when ICAM-1 is highly clustered and immobile on the surface of the target (Gross et al., 2010). Collectively, these studies indicate that ICAM-1 mobility impacts integrin-based adhesion and signaling, and suggest that modulation of ICAM-1 mobility on the APC surface may be an important variable in T cell activation.

The importance of actin dynamics on the T cell side of the IS is well established, but much less is known about the function of the dendritic cell (DC) F-actin network. DC maturation in response to inflammatory stimuli is associated with increased F-actin content and controlled changes in actin regulatory proteins. For example, LPS-induced maturation leads to robust upregulation of the actin-bundling protein fascin (Ross et al., 2000) and activation of the severing protein cofilin (Verdijk et al., 2004). In addition to regulating antigen uptake and migration, it is becoming clear that the DC cytoskeleton functions to promote signaling events at the IS. F-actin and actin-binding proteins such as fascin reportedly accumulate at the IS (Al-Alwan et al., 2003), and treatment of DCs with actin-depolymerizing agents impairs their ability to prime T cell responses (Al-Alwan et al., 2001). Exactly how the DC cytoskeleton promotes T cell priming is unclear. One proposed mechanism involves T cell capture, a process that relies on signaling through Rho family GTPases (Benvenuti et al., 2004). In keeping with this, DCs deficient for the Rho GTPase effector WASp exhibit fewer and shorter-lived contacts with cognate T cells, and a diminished ability to prime T cell proliferation (Bouma et al., 2011).

We now show that maturation-associated changes in the DC actin cytoskeleton function to restrain ICAM-1 lateral mobility, a process that promotes affinity maturation of LFA-1 on interacting T cells and lowers the threshold for T cell activation. These findings reveal a previously unrecognized function for the actin cytoskeleton at the DC side of the IS, whereby retention forces on T cell ligands modulate mechanosensing and force transduction by their cognate receptors on the T cell surface.

Results

Dendritic cells regulate the lateral mobility of ICAM-1 upon maturation

The DC actin cytoskeleton has been shown to promote T cell priming, but the underlying mechanisms are unknown. In light of growing evidence that TCR and integrin activation at the IS involves mechano-transduction (Kim et al., 2009; Li et al., 2010; O'Connor et al., 2012; Springer and Dustin, 2012), we reasoned that the DC cytoskeleton may promote the activation

Downloaded from http://rupress.org/jcb/article-pdf/208/4/457/1586664/jcb_201406120.pdf by guest on 08 February 2026

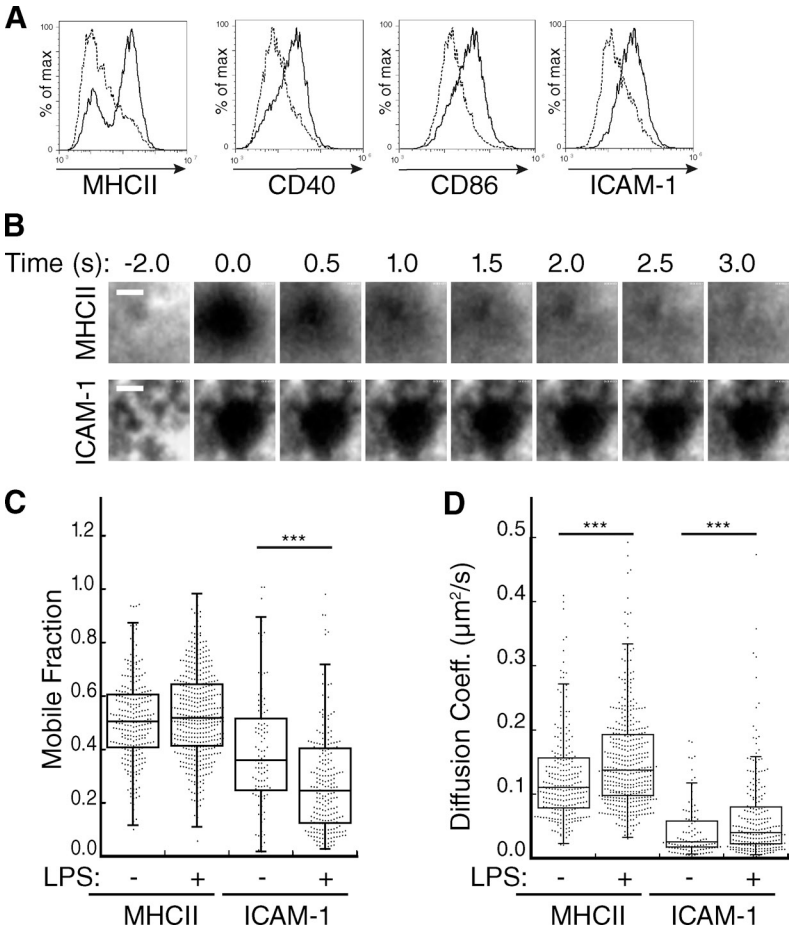

Figure 1. **Dendritic cells regulate the lateral mobility of ICAM-1.** (A) BMDCs were untreated (broken lines) or treated (solid lines) with 100 ng/ml LPS to induce maturation, stained for the indicated proteins, and analyzed by flow cytometry. Data are representative of three individual experiments. (B) Representative images of BMDCs labeled with Fabs against MHCII or ICAM-1 and imaged at the indicated times after photobleaching at time = 0. Bars, 1 µm. (C and D) Mobile fraction (C) and diffusion coefficient (D) of MHCII and ICAM-1 on the ventral surface of control or LPS-matured BMDCs. Dots represent individual FRAP measurements (n = 102–433) pooled from at least three independent experiments. ***, $P < 0.0001$.

of these receptors by constraining the mobility of their cognate ligands. To test this idea, we cultured mouse bone marrow–derived DCs (BMDCs), and incubated them in the absence or presence of LPS to induce maturation, as verified by increased surface expression of MHCII, ICAM-1, CD40, and CD86 (Fig. 1 A). BMDCs were then surface labeled with fluorescent Fab fragments that recognize MHCII or ICAM-1, and lateral mobility of MHCII and ICAM-1 on the plasma membrane was analyzed using FRAP, as detailed in Fig. S1. As shown in Fig. 1 B, MHCII recovered rapidly while ICAM-1 recovery was minimal. Quantitative analysis showed that the mobile fraction of MHCII does not change significantly upon maturation (median values were 0.51 and 0.52 in immature and mature DCs, respectively; Fig. 1 C). The diffusion coefficient (which reflects only mobile molecules) was modestly increased upon maturation, from 0.110 µm^2/s in immature cells to 0.138 µm^2/s in mature cells (Fig. 1 D). These values for MHCII mobility are in good accord with previous findings in B cells (Treanor et al., 2010), and are in the range expected for a freely diffusible membrane protein of this size. In contrast with the high mobility observed for MHCII, ICAM-1 mobility was highly constrained in immature DCs (median value 0.36), and was decreased to 0.25 upon maturation. The diffusion coefficient of the small mobile pool of ICAM-1 molecules increased modestly after LPS treatment, from 0.025 to 0.040 µm^2/s, though values remained significantly lower than those observed for MHCII. Collectively, these data show that in addition to up-regulating the expression of T cell ligands, DC maturation leads to protein-specific changes in ligand mobility.

The DC cytoskeleton clusters ICAM-1 and constrains its lateral mobility

To ask if the DC cytoskeleton controls lateral mobility of MHCII and ICAM-1, we first examined the distribution of these molecules on the DC membrane before and after treatment with actin-depolymerizing agents. In untreated cells, MHCII was relatively evenly distributed over the cell surface, whereas ICAM-1 exhibited a highly clustered, punctate distribution (Fig. 2 A). Treatment with Latrunculin B (LATB) led to complete depletion of the F-actin network, whereas Cytochalasin D (CytoD) induced the accumulation of disordered F-actin–rich zones. Neither drug had a noticeable effect on the distribution of MHCII, but both induced a more homogeneous distribution of ICAM-1, with loss of the punctate organization. FRAP analysis revealed that disruption of F-actin also induced a significant increase in the mobile fraction of ICAM-1 (Fig. 2 B). This effect was specific to ICAM-1; MHCII exhibited a decrease in the mobile fraction upon actin depolymerization, the magnitude of which was inhibitor specific. Inhibitors had a minimal effect on the diffusion coefficient of either protein (Fig. 2 C). The increased mobile fraction of ICAM-1 is consistent with its redistribution on the

Downloaded from http://rupress.org/jcb/article-pdf/208/4/457/1586664/jcb_201406120.pdf by guest on 08 February 2026

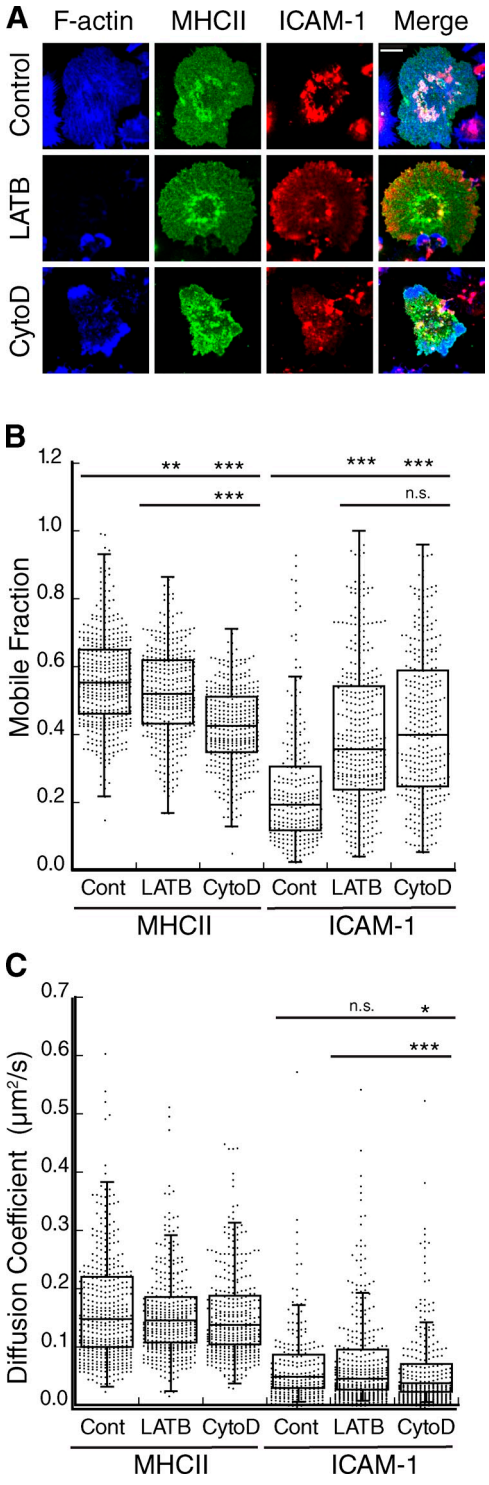

Figure 2. **The DC actin cytoskeleton clusters ICAM-1 and constrains its mobility.** (A) Mature BMDCs were treated with the indicated actin-depolymerizing agents, fixed, and labeled for cell surface MHCII and ICAM-1, followed by permeabilization and labeling for F-actin. Bar, 10 µm. (B and C) Mobile fraction (B) and diffusion coefficient (C) of MHCII and ICAM-1 on mature BMDCs treated as indicated. Dots represent individual FRAP measurements (n = 253–417) pooled from four independent experiments. *, P < 0.01; **, P < 0.001; ***, P < 0.0001.

cell surface shown in Fig. 2 A. Together, these data clearly show that ICAM-1 mobility in mature DCs is selectively constrained by the F-actin network.

ICAM-1 mobility is controlled by interactions with moesin and α-actinin-1

Immobilization of ICAM-1 has been documented in endothelial cells, where it has been shown to depend upon binding of the ICAM-1 cytoplasmic tail to actin-binding proteins of the ERM and α-actinin families (Carpén et al., 1992; Barreiro et al., 2002; Celli et al., 2006; Oh et al., 2007). We therefore tested the expression patterns of these proteins in DCs. As shown in Fig. 3 A, immature BMDCs express the ERM family members moesin and ezrin in an ∼8:1 ratio. Upon maturation, moesin expression was up-regulated, and a greater proportion was in the active form, as measured by phosphorylation at T558. This effect was clearly detectable after 24 h, and by 48 h mature DCs expressed 10-fold more active moesin than immature DCs. No change in the expression or phosphorylation of ezrin was observed. In addition to moesin, nonmuscle α-actinin was also expressed and was slightly up-regulated after LPS treatment (Fig. 3 B).

Immunofluorescence microscopy of mature DCs showed that the puncta containing high levels of cell surface ICAM-1 colocalize with sites of moesin enrichment (Fig. 3 C, inset). MHCII and moesin did not colocalize (Fig. 3 D), which suggests a specific moesin–ICAM-1 interaction. In addition to colocalizing on the ventral surface of DCs, moesin and ICAM-1 were also observed to cap on one side of DCs, when imaged through a midplane (Fig. 3 E).

To ask if moesin and α-actinin-1 control ICAM-1 mobility in BMDCs, we used siRNA to suppress each protein separately or in combination. Moesin expression was reduced by 80%, whereas only a 50% reduction in α-actinin 1 could be achieved (Fig. 3 F). This may reflect residual expression of α-actinin 1, or the presence of α-actinin 4 (the available antibody detects both isoforms). As shown in Fig. 3 G, suppression of either moesin or α-actinin 1 alone resulted in an increase in the mobile fraction of ICAM-1, and simultaneous suppression of both proteins had an additive effect. This change was accompanied by a small, but statistically significant decrease in the diffusion coefficient of ICAM-1 (Fig. 3 H). These changes were specific for ICAM-1; MHCII mobility was unaltered by suppression of moesin and/or α-actinin. Interestingly, we noticed that when DCs were cultured in a cocktail containing both GM-CSF and IL-4, moesin was heavily phosphorylated before LPS treatment (Fig. S2 A). This correlated with a low level of ICAM-1 mobility in immature cells (Fig. S2, B and C), thus implicating moesin activation as a key element controlling ICAM-1 mobility. Collectively, these data indicate that maturation-dependent changes in actin-binding proteins modulate the lateral mobility of specific molecules on the DC surface.

The intracellular tail is critical for regulation of ICAM-1 mobility in DCs

To determine if interactions between moesin/α-actinin-1 and the ICAM-1 cytoplasmic tail control ICAM-1 mobility, we created an ICAM-1 mutant lacking most of the cytoplasmic tail, including the conserved polybasic region proposed to interact with moesin and α-actinin-1 (Oh et al., 2007; Fig. 4 A). BMDCs

Downloaded from http://rupress.org/jcb/article-pdf/208/4/457/1586664/jcb_201406120.pdf by guest on 08 February 2026

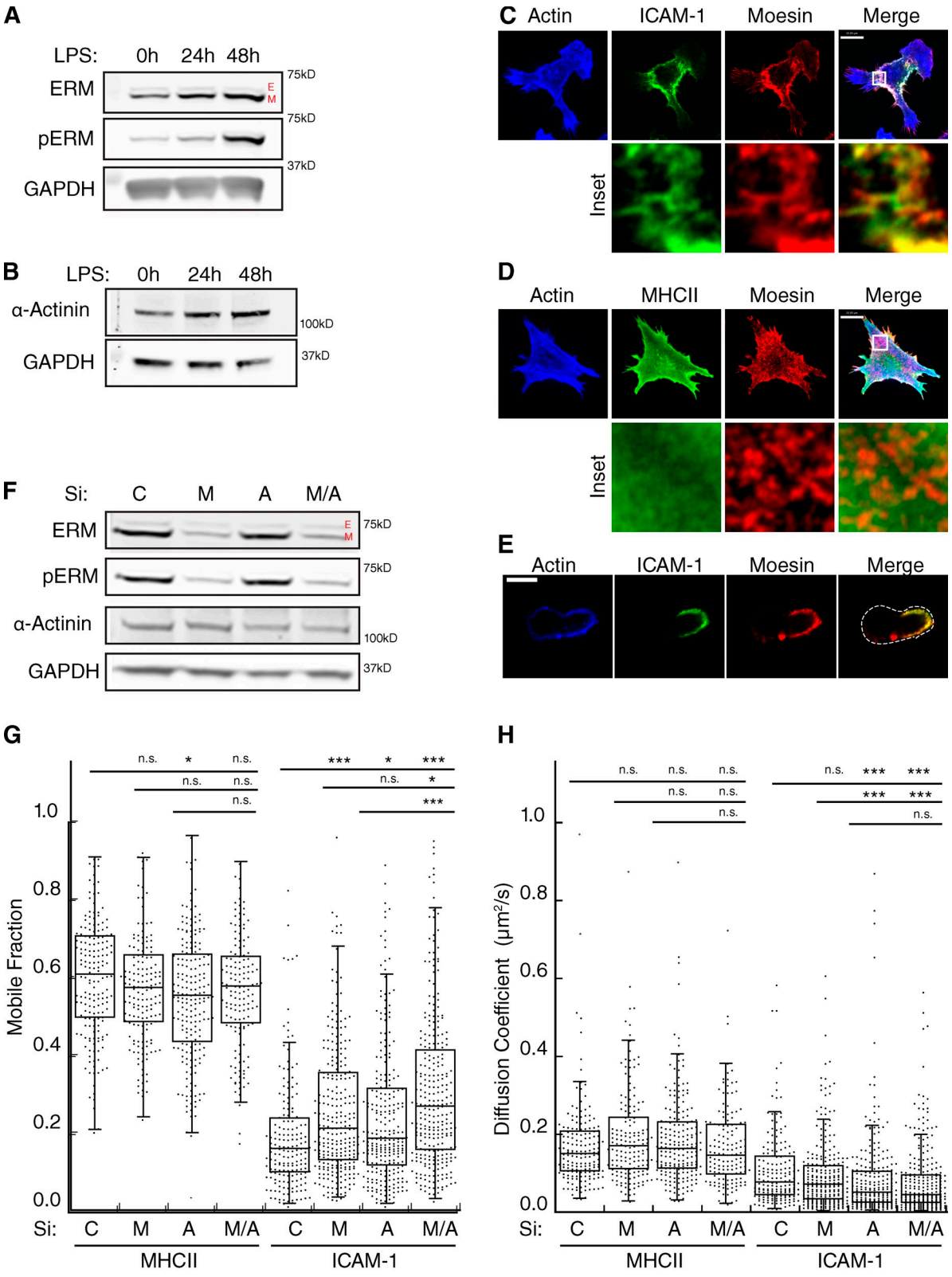

Figure 3. **Actin regulatory proteins moesin and α-actinin-1 regulate the lateral mobility of ICAM-1.** (A and B) Western blots showing levels of total and phosphorylated ERM proteins (A) and α-actinin1 in lysates from BMDCs matured with 100 ng/ml of LPS for 24 or 48 h (B). E, ezrin; M, moesin. (C and D) Immunofluorescence micrographs showing the distribution of F-actin and moesin with respect to cell surface ICAM-1 (C) or MHC II (D). Bottom panels show enlarged regions indicated by the white boxes. (E) Midplane of cell prepared as in C, demonstrating co-capping of ICAM-1 and moesin. (F) Western blot showing siRNA-mediated knockdown of either moesin (M), α-actinin 1 (A), or both proteins (M/A) in mature BMDCs. (G and H) Mature BMDCs treated with siRNA as in F were surface labeled with Fabs against MHCII or ICAM-1, and FRAP analysis was performed to determine the mobile fraction (G) and diffusion coefficient (H). Dots represent individual FRAP measurements (n = 143–285) pooled from three independent experiments. *, $P < 0.01$; ***, $P < 0.0001$. Bars, 10 μm.

Downloaded from http://rupress.org/jcb/article-pdf/208/4/457/1586664/jcb_201406120.pdf by guest on 08 February 2026

from ICAM-1$^{-/-}$ mice were then lentivirally transduced with either wild-type (WT) ICAM-1 or the ΔTail mutant (Fig. 4 B), and lateral mobility was compared with endogenous ICAM-1 in WT C57BL/6-derived BMDCs. Reconstituted WT ICAM-1 exhibited a higher mobile fraction than the endogenous protein, but a similar diffusion coefficient, possibly due to the overexpression of the reconstituted protein (Fig. 4, C and D). When compared with reconstituted WT ICAM-1, the ΔTail mutant exhibited a significantly higher mobile fraction and diffusion coefficient, despite expression levels similar to endogenous ICAM-1. Indeed, both values were consistent with free mobility (compare with freely mobile MHCII in Fig. 1, C and D). To test the effect of anchoring ICAM-1 directly to actin filaments, we created a chimeric molecule in which the cytoplasmic tail was replaced with the flexible linker region and actin-binding domain of moesin (Fig. 4 A). The chimera was expressed well in ICAM-1$^{-/-}$ BMDCs (Fig. 4 B), and demonstrated a mobile fraction below that of reconstituted WT ICAM-1 and similar to endogenous ICAM-1. Not surprisingly, the ΔTail mutant was much more evenly distributed on the DC surface than WT ICAM-1 (Fig. 4 E, quantified in Fig. 4 F). Additionally, ΔTail ICAM-1 did not form a polarized cap as often as WT ICAM-1 (Fig. 4 G). Conversely, the chimeric ICAM-1 was more unevenly distributed than WT protein, and formed caps on the majority of cells (Fig. 4, E–G). Together, these data demonstrate that the limitations of ICAM-1 lateral mobility are almost entirely due to its cytoplasmic domain. Because the chimeric molecule, which can bind directly to actin filaments, shows mobility similar to that of endogenous ICAM-1, this implies that most endogenous ICAM-1 molecules are linked to the actin cytoskeleton. This most likely occurs through the combined action of moesin and α-actinin-1.

Constrained ICAM-1 mobility promotes late events needed for efficient T cell priming

We next asked if immobilization of ICAM-1 on the DC surface is important for T cell priming. ICAM-1$^{-/-}$ DCs were reconstituted with WT ICAM-1 or the ΔTail mutant, or transduced with GFP alone. Upon LPS treatment, these cells expressed similar levels of MHC II, CD40, ICAM-1, and CD86 (Fig. S3 A). Cells were then pulsed with varying doses of $Ova_{323–338}$ peptide and used to prime OTII TCR transgenic T cells. As anticipated, ICAM-1$^{-/-}$ DCs failed to prime T cells as measured by up-regulation of CD25, production of IL-2, or carboxyfluorescein succinimidyl ester (CFSE) dilution (Fig. 5, A–C). Reconstitution with either the WT or ΔTail ICAM-1 constructs rescued CD25 up-regulation (Fig. 5 A) and induced equivalent production of IL-2 at all peptide doses (Fig. 5 B). Though it has been reported that ICAM-1–LFA-1 interactions are important for early IL-2 secretion (Perez et al., 2003), we found no difference in the amount of IL-2 produced at 6, 12, or 18 h, as measured by either ELISA or surface capture (Fig. S3, B–F). Despite their ability to drive early T cell activation events, however, DCs expressing the ΔTail ICAM-1 mutant were not as efficient at stimulating T cell proliferation as DCs expressing exogenous WT ICAM-1 (Fig. 5 C; see also Figs. S3, G–I). This was not an absolute defect, but rather a 1/2 to 1 log shift in the peptide dose response. Quantitative analysis revealed that the defect was primarily due to the failure to undergo multiple rounds of division, rather than initial failure to enter the cell cycle (Fig. 5, D and E). Addition of exogenous IL-2 did not rescue the proliferation defect (Fig. S3, G and H), which is consistent with our observation that IL-2 production and secretion are unaffected.

As a complementary means of liberating ICAM-1 and testing the effects on T cell priming, we interfered with moesin and α-actinin function. Initial efforts based on siRNA-mediated suppression proved uninterpretable because suppression did not last for the duration of T cell priming experiments (unpublished data). We therefore expressed the moesin FERM domain, a dominant-negative mutant that dissociates endogenous ERM proteins from cortical binding partners (Allenspach et al., 2001). The FERM domain increased ICAM-1 mobility, and diminished conjugation and T cell priming, including early events not affected by mutation of the ICAM-1 tail (Fig. S4). However, these results must be interpreted with caution, as this construct also perturbed expression of MHCII and CD86.

Collectively, our findings are consistent with a model in which constrained ICAM-1 mobility promotes late events needed for optimal T cell activation. However, we considered the alternate possibility that the defect in T cell proliferation is the result of defects in ICAM-1–mediated signaling in the DC. ICAM-1 signaling is best studied in endothelial cells, where it depends on phosphorylation of tyrosine 518 in the ICAM-1 tail (Liu et al., 2012). To ask if similar events are required for T cell priming, we mutated tyrosine 518 to phenylalanine (Fig. 4 A). Transduced ICAM-1$^{-/-}$ BMDCs expressed similar levels of Y518F and WT ICAM-1, and these molecules showed similar mobility (Fig. 4, C and D), and stimulated T cell proliferation equally well (Fig. 5 F). Thus, the requirement for the ICAM-1 cytoplasmic tail most likely involves regulation of mobility rather than downstream signaling to the DC.

Constrained ICAM-1 mobility promotes conjugate formation and T cell homotypic interactions

Because ICAM-1 functions as the primary ligand for LFA-1–dependent T cell adhesion, we next asked if ICAM-1 mobility is important for T cell–DC conjugation. As shown in Fig. 5 G, T cells failed to bind to ICAM-1$^{-/-}$ DCs, and this defect was rescued by reconstitution with WT ICAM-1. In contrast, ΔTail ICAM-1 supported significantly less T cell binding; conjugation efficiency was only ∼50% of that obtained with WT-ICAM-1 reconstituted DCs. Because the chimeric ICAM-1 molecule showed diminished lateral mobility, we also asked if DCs expressing this mutant would show enhanced T cell binding. For reasons that are unclear, however, conjugation frequency for these cells varied widely, and was sometimes as low as the ICAM-1$^{-/-}$ controls (Fig. S3 J). Nonetheless, the chimera consistently failed to rescue T cell proliferation (Fig. S3 I), even in experiments where conjugate formation occurred with high frequency. This result may demonstrate the need to actively redistribute ICAM-1 on the surface of DCs through transient changes in moesin activity, analogous to the process that has

Downloaded from http://rupress.org/jcb/article-pdf/208/4/457/1586664/jcb_201406120.pdf by guest on 08 February 2026

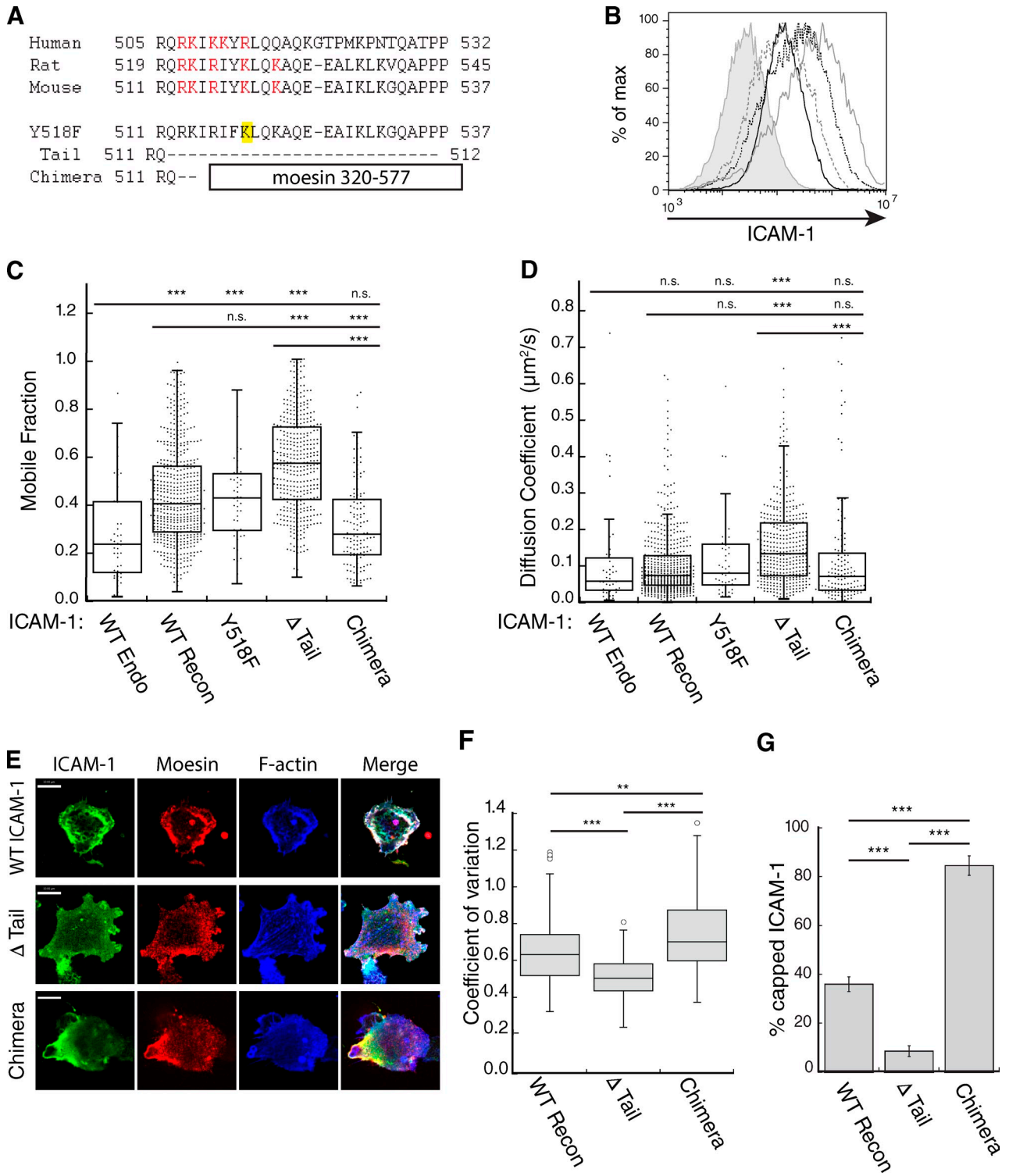

Figure 4. **The cytoplasmic tail of ICAM-1 mediates clustering and lateral mobility in the plasma membrane of BMDCs.** (A) Sequence alignments of the ICAM-1 cytoplasmic tail and ICAM-1 constructs. (B) ICAM-1$^{-/-}$ BMDCs were transduced with ICAM-1 mutants, and cell surface levels were compared by flow cytometry. ICAM-1$^{-/-}$ cells (shaded gray line), WT cells expressing endogenous ICAM-1 (solid black line), ICAM-1$^{-/-}$ cells reconstituted with WT (solid gray line), Δ Tail (broken gray line), or chimera (broken black line) constructs. Results are representative of three individual experiments. (C and D) Mobility of endogenous ICAM-1 and exogenous ICAM-1 mutants expressed in ICAM-1$^{-/-}$ BMDCs was analyzed using FRAP. (C) Mobile fraction; (D) diffusion coefficient. Dots represent individual FRAP measurements (n = 42–523). Data were pooled from five independent experiments except for endogenous, which was pooled from two experiments, and Y518F, which was from a single experiment. (E) Immunofluorescence microscopy showing the distribution of moesin and F-actin with respect to ICAM-1 in LPS matured ICAM-1$^{-/-}$ BMDCs reconstituted with exogenous WT, Δ Tail, or chimeric ICAM-1. Bars, 10 μm. (F) Images collected as in E were analyzed for ICAM-1 clustering by measuring the coefficient of variation (standard deviation/mean) of surface ICAM-1 intensity. Data are from one experiment (n = 50 cells) representative of three independent experiments. (G) Capping of exogenous ICAM-1 in transduced DCs was quantified from midplane images similar to Fig. 3 E. Data are means ± standard deviation (error bars) from four replicate coverslips (~50 cells each) in one experiment, representative of two independent experiments. **, P < 0.001; ***, P < 0.0001.

Downloaded from http://rupress.org/jcb/article-pdf/208/4/457/1586664/jcb_201406120.pdf by guest on 08 February 2026

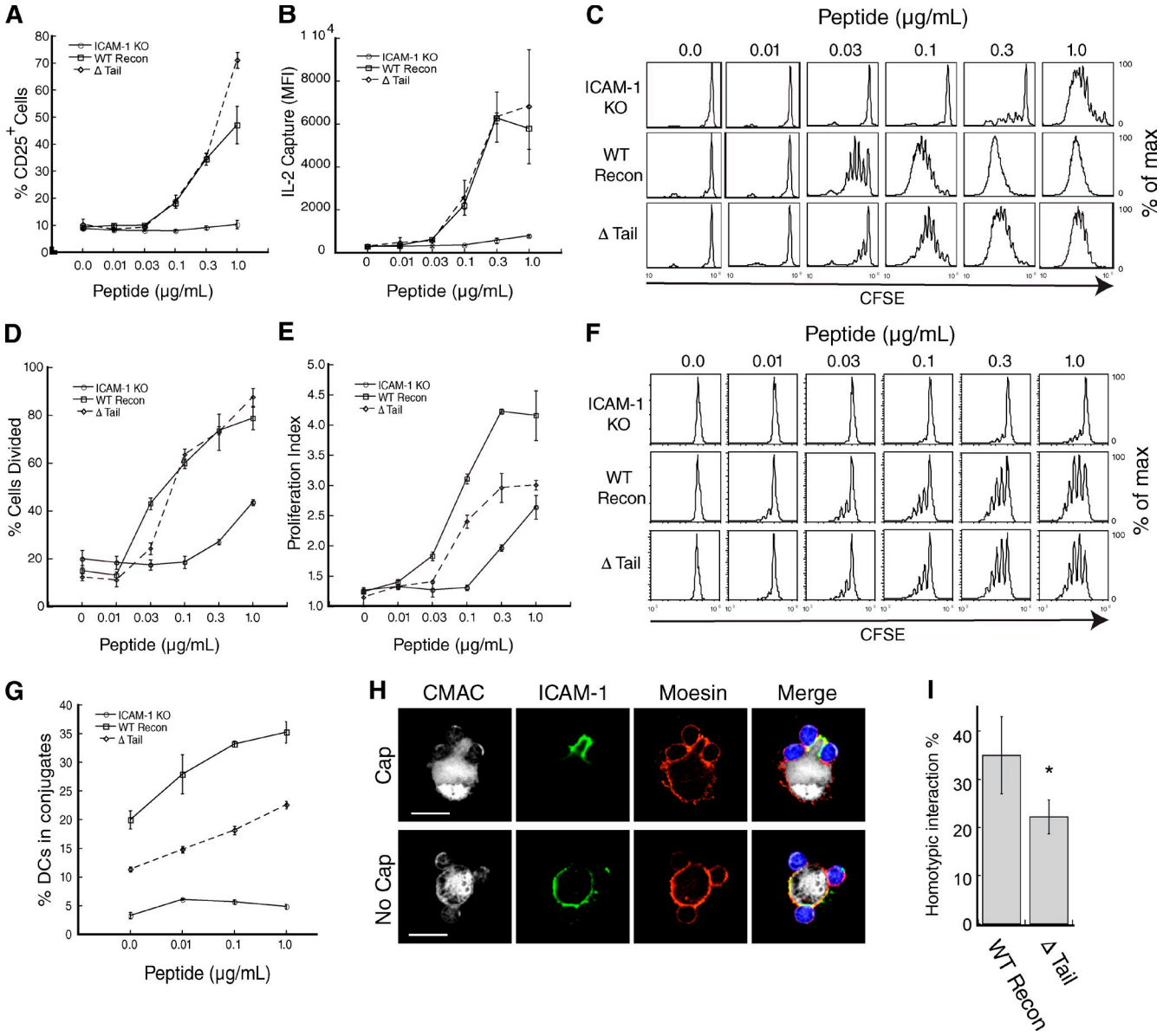

Figure 5. **Altering ICAM-1 mobility perturbs T cell adhesion and priming.** (A) ICAM-1$^{-/-}$ DCs were transduced with GFP or the indicated ICAM-1 constructs, pulsed with peptide at the indicated concentrations, and used to prime CD4^{+} OTII T cells. CD25 surface expression was assessed after 18 h of stimulation. (B) T cells were stimulated as in A and IL-2 secretion was assessed after 18 h using a surface capture assay. (C) CFSE-labeled T cells were stimulated as in A, and CFSE dilution was measured after 96 h to assess proliferation. (D and E) Data were further analyzed to assess the percentage of cells that underwent at least one division (D) and the mean number of divisions of dividing cells (E). Results in A–E are representative of five independent experiments, with data in A, B, D, and E showing mean ± standard deviation (error bars) from triplicate samples in one representative experiment. (F) T cell proliferation was assessed after priming with ICAM-1$^{-/-}$ DCs or ICAM-1$^{-/-}$ DCs transduced with WT ICAM-1 or the signaling-incompetent Y518 mutant. Results are representative of three independent experiments. (G) Conjugate formation was assessed by flow cytometry. Data shown are mean ± standard deviation (error bars) from triplicate samples in one experiment, representative of four individual experiments. (H) Representative midplane images showing T cells interacting with DCs that do or do not display capped ICAM-1. Bars, 10 µm. (I) Conjugates were prepared and imaged as in F. DCs interacting with two T cells were randomly selected and scored for homotypic T cell interactions. Data represent means ± standard deviation (error bars) from four independent experiments, with at least 50 cells each. *, $P < 0.05$.

been documented for CD43 on the T cell side of the IS (Allenspach et al., 2001; Delon et al., 2001).

After DC binding, responding T cells form homotypic interactions, which augment T cell activation by allowing paracrine signaling of IL-2 and IFN-γ (Sabatos et al., 2008; Gérard et al., 2013). These stable homotypic interactions occur at preformed areas enriched in microvilli (Fisher et al., 2008). Because ERM proteins organize microvilli, we reasoned that these T cell "docking sites" might correspond to the capped regions enriched in moesin and ICAM-1 (Fig. 3 E). In support of this idea, we frequently observed clusters of T cells in association with moesin/ICAM-1–rich caps (Fig. 5 H, top). To test if ICAM-1 mobility and interaction with moesin are important for maintaining homotypic T cell contacts, T cells were allowed to interact with DCs expressing either WT or ΔTail ICAM-1, and randomly selected conjugates were scored for the presence

Downloaded from http://rupress.org/jcb/article-pdf/208/4/457/1586664/jcb_201406120.pdf by guest on 08 February 2026

of direct T cell–T cell contact. Analysis was restricted to conjugates consisting of one DC and two T cells, to avoid effects of conjugate efficiency per se and to decrease the likelihood of coincidental homotypic T cell contacts. Under these conditions, 35% of DCs reconstituted with WT ICAM-1 showed homotypic T cell interactions (Fig. 5 I). In contrast, and consistent with their inability to form caps, only 22% of DCs expressing the ΔTail ICAM-1 mutant supported homotypic T cell contacts. Collectively, these data show that constrained ICAM-1 mobility promotes the formation of stable T cell–APC conjugates, and that active redistribution of ICAM-1 encourages T cell homotypic interactions. Both of these processes probably contribute to lowering the antigen threshold for T cell proliferation.

LFA-1 affinity regulation is strengthened by restriction of ICAM-1 lateral mobility

The conformational changes associated with LFA-1 activation are thought to involve force on the ICAM-1–LFA-1 bond, exerted by the T cell actin cytoskeleton (Schürpf and Springer, 2011; Springer and Dustin, 2012; Kong et al., 2013). If so, we reasoned that constraining lateral movement of ICAM-1 could serve to enhance this process by providing resistance on the APC side of the IS. To test this idea, we took advantage of a panel of antibodies specific for conformational intermediates of human LFA-1 (Fig. 6 A, top; Schürpf and Springer, 2011). As surrogate APCs, we generated 293T cell lines stably expressing ICAM-1 variants and functionalized the plasma membranes with αCD3, as detailed in Materials and methods and diagrammed in Fig. 6 A (bottom). FRAP analysis confirmed that the variants behaved in 293T cells as they did in DCs; i.e., they showed low mobility (Chimera), medium mobility (WT), and high mobility (ΔTail; Fig. 6, B and C). Human peripheral blood $CD4^+$ T cells were then allowed to spread on these artificial APCs, and labeled for LFA-1 conformational intermediates. The addition of ICAM-1 to αCD3-functionalized 293T cells resulted in the adoption of both the intermediate-affinity (marked by Kim127) and high-affinity (marked by m24) conformations. Example images showing antibody labeling are presented in Fig. 6 D.

To assess the relative efficiency of conformational change independently of any changes in cell surface LFA-1 levels, total cell surface labeling for the intermediate- and high-affinity epitopes was normalized to total cell surface LFA-1 (marked by TS2/4). We observed no correlation between adoption of the intermediate conformation and ICAM-1 mobility (Fig. 6 E), but we did observe adoption of the high-affinity conformation, correlated with constraint of ICAM-1 mobility (Fig. 6 F). Compared with T cells stimulated with APCs expressing WT ICAM-1, T cells stimulated on APCs expressing the high-mobility ΔTail ICAM-1 showed reduced LFA-1 conformational change, whereas those stimulated on APCs expressing the low-mobility chimera showed increased conformational change. We also tested this question using resting T cell blasts, as blasts typically have more basally activated integrins than naive cells. Again, we found no relationship between ICAM-1 mobility and the intermediate conformation of LFA-1 (Fig. 6 G), whereas in two separate donors we found that the adoption of the high-affinity conformation correlated inversely with ICAM-1 mobility (Fig. 6, H and I). Consistent with our findings for conjugate formation and T cell proliferation, the effect of liberating ICAM-1 from mobility constraints was not all-or-nothing. The 293T cells expressing the ΔTail mutant did support some change to the high-affinity conformation above nontransduced 293T cells, though in two of three donors this did not reach statistical significance.

The inverse correlation between ICAM-1 mobility and LFA-1 conformational change is consistent with a tension-based model, but cytoskeletal constraint of ICAM-1 can also influence local concentrations, and it has been shown that ligand binding can induce LFA-1 conformational change and m24 epitope exposure (Dustin, 1998). Thus, it was important to assess the possible effects of differences in ligand density among our artificial APCs. Analysis of ICAM-1 density on the artificial APCs (Fig. S5) shows that the efficiency of LFA-1 conformational change did not depend on ICAM-1 expression levels; two clones expressing 20-fold different levels of WT ICAM-1 induced the same amount of high-affinity LFA-1. Moreover, cells expressing the Δ-tail mutant at high levels still yielded the lowest amount of high-affinity LFA-1.

Together with our findings from the conjugate assay, these results support a model in which regulation of ICAM-1 mobility on mature DCs serves to facilitate integrin activation on responding T cells, leading to firm adhesion and enhanced T cell priming (Fig. 7).

Discussion

While actin remodeling on the DC side of the IS is essential for conjugate formation and T cell priming (Al-Alwan et al., 2001; Eun et al., 2006; Bouma et al., 2011), it has been unclear how the DC F-actin network contributes to T cell activation. We now show that in addition to the well-documented up-regulation of T cell stimulatory ligands, DC maturation induces cytoskeletal changes that modulate the mobility of those ligands. In mature DCs, actin-binding proteins constrain ICAM-1 lateral mobility, thereby promoting affinity regulation of LFA-1. This process enhances T cell conjugation, T cell homotypic interactions, and T cell proliferation. Controlled immobilization of DC ligands for mechanosensitive T cell molecules represents a novel mechanism by which the DC actin cytoskeleton enhances the potency of DCs as APCs.

Integrin-dependent adhesion is regulated at two levels: affinity (the strength of each individual bond) and valency (the total number of bonds). The product of the two factors gives avidity, or the total strength of the system (Kinashi, 2005). Our work shows that both regulatory mechanisms are impacted by interaction of integrin ligands with the APC cytoskeleton. With respect to affinity, we find that modulation of ICAM-1 mobility aids LFA-1 conformational change and T cell adhesion. Active LFA-1 is linked to the T cell actin cytoskeleton (Cairo et al., 2006), and has been predicted to undergo force-dependent conformational change driven by the T cell actin network (Zhu et al., 2008; Schürpf and Springer, 2011; Springer and Dustin, 2012). Moreover, the bond lifetime of ICAM-1 and LFA-1 increases

Downloaded from http://rupress.org/jcb/article-pdf/208/4/457/1586664/jcb_201406120.pdf by guest on 08 February 2026

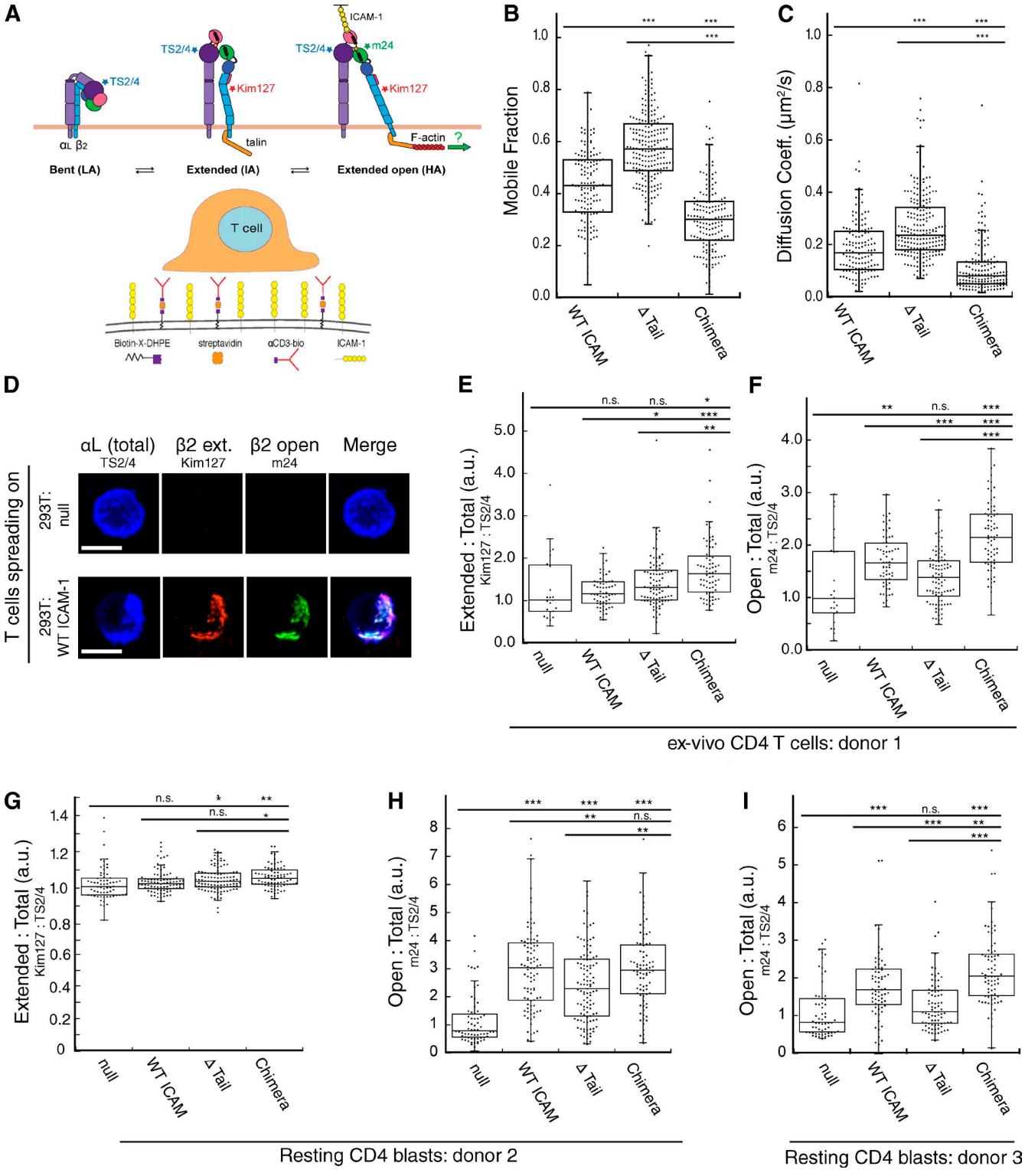

Figure 6. **Restriction of ICAM-1 lateral mobility promotes LFA-1 affinity maturation.** (A, top) Diagram of LFA-1 conformational states with conformation-specific mAb binding sites. (A, bottom) Schematic showing 293T cell–based artificial APCs used to stimulate T cells, as detailed in the Materials and methods. (B and C) Mobile fraction (B) and diffusion coefficient (C) of ICAM-1 in 293T artificial APCs. Dots represent individual FRAP measurements (n = 140–215) pooled from three independent experiments. (D) Ex vivo human T cells were allowed to interact with artificial APCs lacking ICAM-1 (null) or transduced with WT ICAM-1. Conjugates were fixed and labeled with conformation-specific anti–LFA-1 antibodies. Representative micrographs are shown. Bars, 10 µm. (E and F) Conjugates were prepared as in D. (E) The relative proportion of LFA-1 in the extended conformation was assessed based on the ratio of Kim127:TS2/4 labeling intensity. (F) The relative proportion of LFA-1 in the extended open conformation was assessed based on the ratio of m24:TS2/4 labeling intensity. (G–I) Conjugates were prepared and analyzed as in D–F, except that resting T lymphoblasts were used. H and I show T cells from two different human donors in order to show reproducibility. Dots in E–I represent values from single cells (n = 22–107 cells per condition) pooled from two independent experiments (E and F) or three independent experiments (G–I). *, P < 0.05; **, P < 0.001; ***, P < 0.0001.

Downloaded from http://rupress.org/jcb/article-pdf/208/4/457/1586664/jcb_201406120.pdf by guest on 08 February 2026

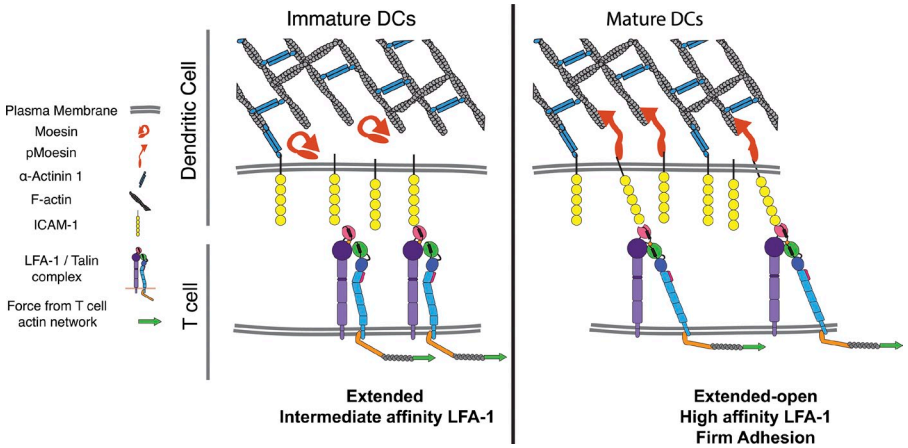

Figure 7. **Model showing how DCs regulate ICAM-1 mobility to enhance LFA-1 activation on T cells.** (left) In immature DCs, levels of active moesin and α-actinin are low, allowing significant lateral mobility of ICAM-1. Upon maturation (right), moesin and α-actinin are up-regulated and activated, leading to immobilization of ICAM-1 via interactions between the cytoskeleton and the ICAM-1 cytoplasmic tail. Low-mobility ICAM-1 provides increased resistance to forces applied to the LFA-1 β-chain by the T cell actin cytoskeleton. This process promotes LFA-1 tail separation, and conformational changes in the extracellular domain associated with increased affinity for ICAM-1. Ultimately, these events lead to increased adhesion and T cell activation.

with force (Kong et al., 2009, 2013; Chen et al., 2010a). TCR-induced inside-out signaling is not sufficient to induce the high affinity conformation of LFA-1, and surface-bound ligands support the high affinity LFA-1 conformation much more efficiently than soluble ligands (Feigelson et al., 2010). In the accompanying paper, we have directly tested the effects of T cell actin cytoskeletal dynamics on LFA-1 conformational change (see Comrie et al. in this issue). We show that ongoing centripetal flow of the T cell actin network is required to maintain LFA-1 in the high-affinity conformation at the IS, and that mobility of ICAM-1 on artificial stimulatory surfaces influences the organization of active LFA-1 molecules on the surface of interacting T cells. In light of those findings, it makes sense that constraints on ICAM-1 mobility mediated by the DC cytoskeleton would oppose F-actin flow on the T cell side of the IS, thereby maximizing the mechanical force on LFA-1.

Interactions between ICAM-1 and the DC actin cytoskeleton also affect integrin valency. We show that ICAM-1 is maintained in a clustered state, both at the submicron scale and in higher order "caps" at one pole of the DC, where T cells preferentially bind. Importantly, high local concentrations of ICAM-1 may also contribute to affinity modulation through an "induced fit" mechanism (Cabañas and Hogg, 1993; Dustin, 1998; Zhu et al., 2013). Indeed, we have found that full LFA-1 activation requires both tension and ligand binding (Comrie et al., 2015). Though we did not observe a correlation between the global ICAM-1 expression level and LFA-1 conformational change, submicron-scale clustering may still be important, particularly under physiological conditions where ICAM-1 is limiting.

We find that lateral mobility of ICAM-1 is regulated by maturation-induced up-regulation and activation of moesin and α-actinin through a mechanism involving the cytoplasmic domain of ICAM-1. It is currently unclear whether ICAM-1 mobility is limited by direct tethering or by molecular fences that confine diffusion. The two mechanisms are not mutually exclusive, and there are precedents for both. Direct binding of ICAM-1 to both ezrin and α-actinin has been demonstrated in endothelial cells (Carpén et al., 1992; Celli et al., 2006; Oh et al., 2007). In B cells, moesin has been shown to create cytoskeletal corrals that confine B cell receptor diffusion (Treanor et al., 2010). Two pieces of evidence lead us to favor direct tethering. First, we observe close colocalization of ICAM-1 and moesin. Second, and more importantly, reconstituted WT ICAM-1, which is overexpressed ∼10-fold, is more mobile than the endogenous protein. This phenomenon is consistent with saturation of direct tethers, but would not be expected in a corral-based mechanism. Single-particle tracking studies will be needed to resolve this question with certainty.

Cytoskeletal regulation of ICAM-1 mobility is likely to be of general importance for immune responses that require firm adhesion. In keeping with our findings, Gross et al. (2010) have shown that increasing ICAM-1 mobility in target cells leads to decreased NK cell conjugate formation and granule polarization, whereas decreasing ICAM-1 mobility by overexpression of ezrin has the opposite effect (Gross et al., 2010). Moreover, in endothelial cells, interruption of ICAM-1 interactions with α-actinin and ezrin inhibits the ability of T cells to undergo diapedesis (Celli et al., 2006; Oh et al., 2007).

We show that deletion of the ICAM-1 tail leads to enhanced mobility, which correlates with diminished LFA-1 conformational change, conjugate formation, and T cell priming. Although we attribute the observed functional effects to changes in ICAM-1 mobility, it is important to consider other known functions of the ICAM-1 cytoplasmic tail. First, ICAM-1 could deliver signals to the DC. Where such signals have been studied, they depend Y518 in the ICAM-1 tail (Liu et al., 2012). We show that mutation of this residue has no effect on T cell proliferation. Thus, if signaling is involved, it must use other unknown mechanisms. The ICAM-1 tail can also modulate dimerization. On the cell surface, ICAM-1 exists largely as a homo-dimer formed by interactions in the extracellular and transmembrane regions and opposed by repulsive interactions between conserved basic residues in the cytoplasmic domain (Miller et al., 1995; Yang et al., 2004; Oh et al., 2011). Thus, our tail mutants could affect ICAM-1 dimeric status. This should not affect our results, however, as monomeric and dimeric ICAM-1 show virtually identical affinities for LFA-1 (Jun et al., 2001). Moreover, GPI-anchored ICAM-1 and tailless ICAM-1 (which are largely monomeric and dimeric, respectively) both fail to support LFA-1–mediated adhesion (Miller et al., 1995; Oh et al., 2011). Consistent with our findings, Oh et al. (2011) point out

Downloaded from http://rupress.org/jcb/article-pdf/208/4/457/1586664/jcb_201406120.pdf by guest on 08 February 2026

that both proteins are evenly distributed, and likely highly mobile, compared with WT ICAM-1. The authors concluded that ICAM-1 must be in an intermediate state, between monomer and dimer, that mediates strong adhesion. Given our finding that LFA-1 affinity maturation can be rescued by linking ΔTail ICAM-1 to the actin cytoskeleton in a manner that is unlikely to modulate dimerization or deliver downstream signals, we deem it more likely that T cell adhesion and priming are modulated by changes to ICAM-1 mobility than by changes in dimerization or signaling.

LFA-1 serves a dual purpose at the IS, functioning primarily as an adhesion molecule that stabilizes conjugate formation, but also as a co-stimulatory molecule, adding or augmenting signals that induce T cell activation (Perez et al., 2003; Wang et al., 2008). Importantly, the high-affinity conformation of integrins generally represents the signaling-competent form (Zhu et al., 2007; Lefort et al., 2009). Thus, in addition to enhancing adhesion, ICAM-1 mobility constraint would be expected to increase co-stimulatory signaling. Testing this idea biochemically has proven to be challenging, largely because outside-in signaling by integrins overlaps with and requires TCR signals. Nonetheless, this concept is in line with the finding that ΔTail ICAM-1 can support up-regulation of CD25 and IL-2, but does not support full T cell proliferation, a late event that may be particularly dependent on co-stimulation. It remains to be seen if other effector functions of activated T cells are altered by stimulation with mobile versus immobile ICAM-1 bearing DCs.

Though the APC has largely been regarded as a passive partner during IS formation, there is compelling evidence that it plays an active role in organizing IS structure. The classical "bull's-eye" IS structure occurs in T cell–B cell conjugates, and in T cells spreading on supported planar lipid bilayers (Monks et al., 1998; Grakoui et al., 1999). In contrast, T cells interacting with DCs generally form "multifocal" synapses characterized by multiple patches of CD3 and LFA-1 with variable overlap (Brossard et al., 2005; Reichardt et al., 2007; Thauland and Parker, 2010). The multifocal synapse has been suggested to arise from either topological or cytoskeletal barriers to diffusion (Dustin et al., 2006). We now show that ICAM-1 is, indeed, subject to actin-dependent diffusional barriers, whereas MHCII is not. Despite the lack of cytoskeletal mobility constraints, MHCII and TCR do not form a well-organized central supramolecular activation cluster (cSMAC) in T cell–DC conjugates (Brossard et al., 2005; Thauland and Parker, 2010). Thus, topological barriers may also play a role. Interestingly, moesin helps to form microvilli, structures that have been observed on the DC side of the IS (Bretscher et al., 2002; Fisher et al., 2008). Thus, moesin could form both cytoskeletal barriers for ICAM-1 and topological barriers for other proteins, including MHCII. It will be interesting to ask if moesin function is required for maintenance of the multifocal synapse in DC–T cell conjugates, and if so, how B cells differ in this regard.

Whether or not moesin organizes the multifocal synapse, we found that moesin does organize higher-order adhesive caps on the DC surface, where T cells preferentially bind and contact one another. Similar clusters of T cells contacting DCs have been observed by multiphoton imaging in vivo, even prior to T cell proliferation (John et al., 2009). Recent studies show that homotypic T cell interactions can enhance paracrine signaling via IL-2 and IFNγ, leading to enhanced $CD8^+$ T cell proliferation and memory responses (Sabatos et al., 2008; Steenblock et al., 2011). Homotypic T cell interactions are likely to be particularly important in vivo, where the frequency of responding T cells is low, as well as during $CD4^+$ T cell help with $CD8^+$ T cell priming. It will also be interesting to test this in vivo, and to ask if increasing ICAM-1 mobility shortens interaction times between T cells and DCs. If so, memory formation is likely to be impacted (Scholer et al., 2008).

An important concept arising from our work is that the mobility of individual T cell ligands on the DC surface is regulated independently. Our finding that MHC II is highly mobile has important implications for modeling of TCR-pMHC binding kinetics. Indeed, the differential regulation of ICAM-1 and MHC II mobility allows for efficient activation of LFA-1, while permitting the T cell to scan a large number of pMHC complexes for low frequency antigens. While we focus here on the mobility of ICAM-1, the mechanism that we have uncovered likely applies to other receptor–ligand pairs that modulate T cell activation. In particular, CD80 and CD86 interact with the actin cytoskeleton through motifs similar to those in ICAM-1 (Doty and Clark, 1998; Girard et al., 2012). These motifs control localization of CD80 and CD86, as well as CD28 (Tseng et al., 2005), and deletion of this region impairs co-stimulatory function.

Much remains to be learned about mechanotransduction in T cell activation. We show that biophysical properties of the APC modulate the activation of mechanosensitive molecules. It is likely that the actin cytoskeleton controls not only ligand mobility, but also cortical stiffness, another important parameter for T cell activation (Judokusumo et al., 2012; O'Connor et al., 2012). Further understanding of these processes will be valuable in modulating APC function in therapeutic settings.

Materials and methods

Mice

All mice were obtained originally from The Jackson Laboratory and housed in the Children's Hospital of Philadelphia animal facility, according to guidelines put forth by the Institutional Animal Care and Use Committee. C57BL/6 mice (WT) and ICAM-$1^{-/-}$ mice (B6.129S4-ICAM1^{tm1Jcgr}/J; Xu et al., 1994) were used as a source of bone marrow from which to generate DCs. The ICAM-$1^{-/-}$ strain was generated by insertion of a vector containing the *neo* resistance gene into exon 4 of the *Icam1* gene. T cells were prepared from heterozygous OTII TCR Tg mice, which express a TCR specific for ovalbumin$_{323–339}$ presented on I-A^b (Barnden et al., 1998).

Inhibitors and antibodies

Cytochalasin D and Latrunculin B were from EMD Millipore. Flow cytometry antibodies (rat anti-CD4 APC, Armenian hamster anti-CD11c APC, rat anti-CD40 FITC, rat anti-CD54 Biotin, rat anti-CD54 Alexa Fluor 488, Armenian hamster anti-CD80 FITC, rat anti-CD86 FITC, and rat anti-MHCII Alexa Fluor 488) were from BioLegend. Streptavidin Alexa Fluor 647 was from Invitrogen. A mouse anti-moesin antibody that detects all ERM proteins by Western blotting was from BD (#610401). Rabbit anti-moesin for immunofluorescence microscopy (#3150), a rabbit mAb reactive with an activation-dependent phospho-epitope expressed on all ERM isoforms (pT567 in ezrin, pT558 in moesin; #3149), and rabbit anti–α-actinin (#3134) were all from Cell Signaling Technology. Secondary antibodies for immunofluorescence were from Invitrogen. Mouse anti-GAPDH was from EMD Millipore.

Downloaded from http://rupress.org/jcb/article-pdf/208/4/457/1586664/jcb_201406120.pdf by guest on 08 February 2026

For Fab production, rat antibodies to MHCII (M5/114) and ICAM-1 (YN1/1.7.4) were purchased from Bio X Cell. The Fab preparation kit and immobilized papain and pepsin were from Thermo Fisher Scientific. 1 mg of each antibody was digested for 3 h with immobilized papain according to the manufacturer's protocol. The resulting mixtures of Fab and Fc fragments were then transferred to pepsin digestion buffer by three washes with Ultracel 10 kD centrifugal filters (EMD Millipore), after which Fc fragments were digested by incubation with immobilized pepsin. Samples were then washed three times in 10-kD centrifugal filters and resuspended in PBS. Purity of the resulting Fab preparation was verified by reducing SDS-PAGE and Coomassie R250 staining. Fab fragments were labeled with Alexa Fluor 488 (Invitrogen) according to the manufacturer's protocol. Labeled Fab was tested by flow cytometry to verify intact antigen binding activity.

LFA-1 conformation-specific antibodies

Mouse monoclonal antibodies TS2/4 (anti-CD11a) and Kim127 (anti-CD18) were harvested from hybridomas (ATCC). Mouse monoclonal antibody m24 (anti-CD18) was from Abcam. TS2/4 recognizes an epitope on the β propeller domain of CD11a (αL) only in the assembled αβ heterodimer (Huang and Springer, 1997), and binds in an activation-independent manner (Chen et al., 2006). Kim127 binds to an epitope within the EGF2 domain of CD18 (β2) that is hidden in bent, inactive integrins and exposed upon integrin extension and activation. Kim127 therefore reports on the extended and extended open conformations (Lu et al., 2001; Chen et al., 2006). Because Kim127 is an activating antibody, care was taken to use it only after fixation. m24 binds the activated I domain of CD18 (β2) after hybrid domain swing-out, and therefore reports on the high affinity extended-open conformation of LFA-1 (Dransfield and Hogg, 1989; Chen et al., 2006, 2010b; Schürpf and Springer, 2011). The epitope bound by m24 is sensitive to aldehyde fixation, necessitating prefixation labeling. However, m24 does not induce LFA-1 conformational change. TS2/4 was directly conjugated to DyLight 650, Kim127 was conjugated to Alexa Fluor 594, and m24 was conjugated to Alexa Fluor 488, all according to the manufacturer's protocols. Functionality of antibodies was verified by flow cytometry on unstimulated T cells or cells stimulated with Mn^{2+}.

Cell preparation and culture

Unless otherwise specified, all tissue culture reagents were from Invitrogen/Life Technologies. GM-CSF was produced from the B78H1/GMCSF.1 cell line (Levitsky et al., 1994). To generate BMDCs, leg bones of mice were cleaned of muscle tissues and sterilized in 70% EtOH. Bone marrow was flushed using Iscove's modified Dulbecco's medium (IMDM) containing 1% FBS. Cells were centrifuged at 1,500 rpm at RT for 5 min and resuspended in ACK lysis buffer for 1 min. After washing in IMDM/1% FBS, cells were resuspended in DC culture media (IMDM, 10% FBS, penicillin/streptomycin, GlutaMax, 55 µM β-ME, and 1% GM-CSF supernatant) at a concentration of 10^6 cells/ml. 2 ml of cell suspension was added to wells of 6-well plates and supplemented with 4 ml of DC culture media on day 2. Starting on day 5, 3 ml of media was replaced daily. Differentiation into $CD11c^+$ DCs (typically 70–80%) was verified on day 6 by flow cytometry. To induce maturation, DCs on days 7 or 8 were stimulated with 100 ng/ml LPS (*Escherichia coli* 055:B5; Sigma-Aldrich) for 24–48 h. Maturation was verified by flow cytometry. $OTII^+$ $CD4^+$ T cells were isolated from spleen and lymph nodes by magnetic bead-based depletion (QIAGEN) using anti-CD8 (2.43) and anti-MHCII (M5/114.15.2). T cell activation assays were performed in T cell media (DMEM supplemented with 10% FBS, GlutaMAX, Hepes, NEAA, and β-mercaptoethanol at 37°C and 10% CO_2). HEK-293T cells were cultured in DMEM supplemented with 20 mM Hepes, 10% FBS, 1% GlutaMAX, 1% penicillin/streptomycin, and 1% NEAA.

Human peripheral blood $CD4^+$ T cells were obtained from the University of Pennsylvania's Human Immunology Core under an Institutional Review Board approved protocol. In experiments using ex vivo cells, T cells were used within 3 h of purification. Alternatively, T lymphoblasts were generated by activation with human T-Activator CD3/CD28 magnetic beads (Dynabeads; Life Technologies) in RPMI (Invitrogen) supplemented with 10% FBS (Atlanta Biologicals), 1% GlutaMAX (Invitrogen), 1% penicillin/streptomycin, and 50 U/ml of human rIL-2 (obtained through the AIDS Research and Reference Reagent Program, Division of AIDS, National Institute of Allergy and Infectious Diseases, National Institutes of Health; human rIL-2 was from M. Gately, Hoffmann-LaRoche, Nutley, NJ). T lymphoblasts were cultured in a humidified 37°C incubator with 5% CO_2. Beads were magnetically removed on day 6 after initial stimulation, and cells were then cultured for an additional day in the absence of IL-2.

Plasmid construction, viral production, and transduction of DCs

Lentiviral packaging constructs psPAX2 and PDM2.G as well as Gateway donor vector pDONR221 and destination vector PLX301 were all gifts of N. Hacohen, Broad Institute, Cambridge, MA. Mouse ICAM-1 cDNA was purchased from OriGene. Site-directed mutagenesis was performed using QuikChange (Agilent Technologies). To create the chimeric ICAM-1 molecule, ICAM-1 aa 1–512 (comprising the extracellular and transmembrane domains) were directly fused to mouse moesin aa 320–577 (comprising the flexible linker and actin-binding domains). To create the Moesin dominant-negative (DN) protein, aa 1–320 of mouse moesin was fused at the C terminus to mKate2. WT ICAM-1, ΔTail ICAM-1, T558D ICAM-1, chimeric ICAM-1, Moesin DN-mKate2, and mKate2 sequences were then transferred to the Gateway donor vector, and finally to the destination vector according to the manufacturer's protocol. The HIV-based lentiviral vector pReceiver-Lv105 expressing EGFP (EX-EGFP-Lv105, GeneCopoeia) was used for control transductions.

To generate recombinant lentivirus, 18×10^6 HEK293T cells (ATCC) were seeded in 15-cm plates the day before transfection, and then cotransfected using the calcium phosphate method with 36.3 µg of psPAX2 and 12.1 µg of pDM2.G, together with 48 µg of each DNA of interest (all in PLX301). Supernatants were harvested 30 h after transfection and used immediately to transduce BMDCs. BMDCs were transduced by spin infection with lentivirus on day 1 or 2 of culture. Lentivirus and 8 µg/ml Polybrene (Sigma-Aldrich) were added to the wells of a 6-well culture plate and centrifuged at 2,000 rpm and 37°C for 2 h. Lentivirus-containing media was then replaced with DC culture media, and the cultures were maintained as described as described in the "Cell preparation and culture" section. On day 5 of culture, puromycin (Sigma-Aldrich) was added to a final concentration of 2 µg/ml to select for virally transduced cells. Dead cells were removed by spinning the cell suspension at 2,000 rpm for 15 min on a cushion of Ficoll-Paque Plus (GE Healthcare). Live cells that accumulated at the interface were then collected and washed three times in DC culture media before use.

siRNA-mediated protein suppression

Nontargeting siRNA #2, siRNA SMARTpool against αACTN1, and siMoesin (5′-GGAGCGUGCUCUCCUGGAAUU-3′) were all purchased from GE Healthcare. Electroporation of immature BMDCs was performed on day 6 of culture, followed by LPS maturation on day 7. In brief, 500 pmol total of siRNA was added to 4×10^6 BMDCs at 10^7 cell/ml of Opti-MEM media in a 4-mm gap cuvette (Harvard Apparatus). Cells and siRNA were then electroporated using a ECM830 electroporation device (BTX) with a voltage of 1,000 V and a pulse length of 300 µs, using 2 pulses, with a pulse interval of 500 ms. Cells were then resuspended in DC media lacking GM-CSF for 3 h, after which GM-CSF was added back. Cells were used at day 8 (48 h after electroporation), which was found to be optimal for both moesin and α-actinin.

Flow cytometry

BMDCs were harvested and resuspended at 10^6 cells/ml in ice-cold FACS buffer (PBS, 5% FBS, 0.02% NaN_3, and 1 mM EDTA), 10^5 cells per sample. After incubating for 20 min with the Fc blocking antibody 24G2, cells were washed and resuspended in FACS buffer containing appropriate antibodies and incubated for 30 min on ice. Cells were then washed and resuspended in FACS buffer, and data were collected on a flow cytometer (Accuri C6; BD). Gating was performed based on forward and side scatter (for live cells) and expression of CD11c for DCs. Subsequent analysis was performed on FlowJo (Version 9.5.3). All flow plots are shown on a logarithmic scale for fluorescence intensity.

Fixed cell microscopy

2×10^4 DCs were allowed to spread on 12-mm round coverslips for 1 h at 37°C in DC medium. Cells were fixed in 3% paraformaldehyde in PBS, quenched, permeabilized with 0.1% Triton X-100, and labeled as described previously (Dehring et al., 2011). In brief, cells were washed in PBS with 1% FBS, incubated with primary antibodies sequentially, washed three times in PBS with 1% FBS, and incubated with secondary antibodies. Cells were then washed three times in PBS 1% FBS, twice in PBS, and once in milli-Q H_2O, and mounted on slides with mowiol mounting media (Sigma-Aldrich). To label ICAM-1 or MHCII on the cell surface, cells were incubated with antibodies before permeabilization. Cells were imaged on an inverted microscope (Axiovert 200M; Carl Zeiss) equipped with a spinning disk confocal system (UltraView ERS 6; PerkinElmer) and a 63× Plan-Apochromat 1.4 NA objective lens. Images were collected using an ORCA-ER camera

Downloaded from http://rupress.org/jcb/article-pdf/208/4/457/1586664/jcb_201406120.pdf by guest on 08 February 2026

(Hamamatsu Photonics) using Volocity acquisition software and analyzed using Volocity software (v6.1.1; PerkinElmer).

To analyze ICAM-1 clustering, cells were surface labeled for ICAM-1 and intracellularly labeled for F-actin. The outline of each cell was defined based on F-actin intensity, and the pixel intensity of ICAM-1 labeling across each cell was determined. The coefficient of variation was then calculated by dividing the standard deviation by the mean for each cell.

To analyze T cell–DC interactions, DCs were labeled with CMAC (Invitrogen) incubated for 2 h at 37°C with 1 µg/ml $OVA_{323–339}$ peptide (AnaSpec), and allowed to spread on coverslips for 10 min, at which time CFSE-labeled OTII T cells were added at a 4:1 ratio with DCs and allowed to interact for an additional 50 min. Conjugates were fixed, labeled for surface ICAM-1 and intracellular moesin, and imaged. To analyze homotypic T cell interactions, conjugates of one DC with two T cells were randomly selected and scored for the presence or absence of direct T cell–T cell contact.

FRAP

BMDCs were allowed to spread on eight-chambered cover glasses (Lab-Tek) for 2 h at 37°C in DC media. Slides were then transitioned to 4°C, and fluorescently labeled Fab against MHCII or ICAM-1 was added at 10 µg/ml for 20 min. Labeling media was then removed, and cells were washed and resuspended in prewarmed L15 media (Invitrogen) supplemented with 2 mg/ml glucose. Cover glasses were equilibrated at 37°C on the microscope stage within an environmental chamber and imaged by spinning disk confocal microscopy using the Volocity FRAP plug-in. Before photobleaching, cells were imaged for 3 s at the glass–DC interface at 2 fps. 4–5 randomly selected circular regions/cell (1.7 µm diameter) were then bleached, and images were captured at 2 fps for 20 s for MHCII or 2 fps for 20 s followed by 1 fps for 25 s for ICAM-1. Samples were corrected for photobleaching using the automated feature in Volocity 6.1.1, and FRAP analysis was conducted using the Volocity FRAP Analysis plugin. This software obtains sequential intensity measurements and calculates the mobile fraction (the maximal percentage of initial fluorescence intensity that is recovered by the plateau period) based on the best fit to a single exponential curve constrained through the origin (Sprague and McNally, 2005), the diffusion coefficient based on the half time required to reach maximal recovery ($T_{1/2}$), and the original bleach area diameter (w) using the equation $D = W^2/(4T_{1/2})$ (Axelrod et al., 1976).

For actin depletion experiments, cells were allowed to spread and stained with Fab as before. 15 min before performing photobleaching, Latrunculin B or Cytochalasin D were added to cells at a final concentration of 1 µM or 10 µM, respectively. Inhibitors were added as 5× concentrated solution in prewarmed media. Control cells received an equivalent amount of prewarmed media.

T cell activation assays

2×10^4 DCs were added to each well of a flat-bottom 96-well tissue culture plate and pulsed for 2 h with the indicated amount of $OVA_{323–339}$ peptide. Plates were then spun at 1,500 RPM for 5 min and the media was replaced with fresh T cell media. For proliferation assays, OTII T cells purified by negative selection were labeled with 1 µM CFSE for 5 min at RT. 4×10^4 CFSE-labeled T cells were then added to each well containing peptide-pulsed DCs. Samples were collected after 72–96 h, stained for CD4, and analyzed by flow cytometry. For early T cell activation markers, OTII cells were incubated with an IL-2 capture reagent (Miltenyi Biotec) according to the manufacturer's protocol, and were added to peptide-pulsed BMDCs. After 18 h, cells were washed with FACS buffer, stained with α-CD4 APC, αCD25 Alexa Fluor 488, and αIL-2 PE, and analyzed by flow cytometry. Alternatively, OTII cells were added to DCs, and 100 µl of supernatant was collected at the indicated times and analyzed by ELISA (eBioscience).

T cell–DC conjugation assays

5×10^4 DCs/condition in FACS tubes were pulsed for 2 h with $OVA_{323–339}$ peptide, washed, and resuspended in 200 µl of prewarmed T cell media. 10^5 CFSE-labeled OTII T cells were then added and mixed with DCs. Samples were incubated at 37°C for 45 min, after which anti-CD11c APC was added to a final dilution of 1:500 and incubated for an additional 15 min at 37°C. At 1 h after adding T cells, conjugates were vortexed at max speed for 5 s to break apart loosely adherent cells, fixed in 1% PFA in FACS buffer, and analyzed by flow cytometry. Conjugation efficiency was calculated based on the percentage of CD11c-positive DCs bound to CFSE-labeled T cells.

Generation of artificial APCs and analysis of LFA-1 conformational change

293T cells were transduced with WT, ΔTail, or Chimeric ICAM-1 constructs and selected with 4 µg/ml puromycin. After two rounds of single cell cloning, clones expressing similar levels of exogenous ICAM-1 molecules (within a 10-fold range) were selected and expanded. 18 h before use, 3×10^5 cells were added to 12-mm coverslips (previously acid washed and coated sequentially with 0.1% wt/vol poly-L-lysine [Sigma-Aldrich] for 15 min at RT and 1 µg/ml human fibronectin in PBS [R&D Systems] for 2 h at 37°C). Fusogenic lipid vesicles of DHPE-X-Biotin (Biotium) were prepared by evaporating chloroform from the lipid under vacuum for 0.5–1 h, and dispersal in H_2O at a total lipid concentration of 2 mg/ml. The solution was vortexed for 2 min to create multilamellar liposomes, which were then homogenized in an ultrasonic water bath followed by passing through a 50-µm extruder to create lipid vesicles of homogenous sizes. The vesicle solution was diluted 1:100 in prewarmed 293T cell media and added to the coverslips for 15 min at 37°C. Coverslips were then washed in imaging media (L15 + 2 mg/ml glucose) and incubated with 1 µg/ml streptavidin for 15 min at RT, washed again, and incubated with 10 µg/ml OKT3-Biotin (eBioscience) for 15 min at RT.

After final washing of artificial APCs, 10^5 freshly isolated human peripheral blood $CD4^+$ T cells or resting $CD4^+$ T cell blasts were then added and allowed to adhere for 20 min. Alexa Fluor 488–labeled m24 antibody (final concentration of 4 µg/ml) was added to the coverslips for 5 min at 37°C, after which coverslips were quickly washed in PBS with Ca^{2+}/Mg^{2+} and fixed in 3% PFA. After quenching excess fixative, cells were sequentially surface labeled with Kim127 and TS2/4. T cell–APC conjugates were imaged by confocal microscopy by collecting z stacks that encompassed the cell–cell interface and the entire T cell. Total pixel intensity for each antibody was determined from the rendered images and normalized to T cells responding to APCs lacking ICAM-1. To determine the relative efficiency of LFA-1 conformational change, the ratio of m24 or Kim127 to TS2/4 intensities was determined for each cell.

Western blotting

Cells were washed in cold PBS and lysed at 4°C in 1× RIPA lysis buffer (1% IGEPAL, 0.5% sodium deoxycholate, 0.1% SDS, and 50 mM Tris, pH 7.5), then supplemented with 10 mM NaF, 1 mM Na_3VO_4, and Complete protease inhibitor cocktail (Roche). 10^5 cell equivalents per lane were separated on 4–12% NuPAGE gradient gels (Invitrogen), transferred to nitrocellulose, probed as indicated, and imaged on a fluorescence scanner (Odyssey; LI-COR Biosciences) within the linear range.

Statistical analysis

Statistical analysis was performed using KaleidaGraph software (Synergy). Pairwise comparisons were made using a two-tailed Student's *t* test (for normally distributed data) or a Mann-Whitney test (for nonnormal distributions). Where multiple comparisons were made, a Kruskall-Wallis one-way test for variance was first performed, followed by pairwise Mann-Whitney tests.

Online supplemental material

Fig. S1 details FRAP experimental setup and analysis. Fig. S2 shows the assessment of ERM expression and phosphorylation as well as ICAM-1 mobility in DCs cultured in the presence of IL-4. Fig. S3 shows additional data pertaining to the production and influence of IL-2 during T cell activation as well as data related to T cell conjugation and proliferation in response to Chimeric ICAM-1–expressing DCs. Fig. S4 shows the effects of ERM DN expression in DCs on ICAM-1 lateral mobility and T cell priming. Fig. S5 shows the expression of ICAM-1 in the various 293T-based artificial APCs as well as the comparison of LFA-1 conformational change in T cells responding to low or high ICAM-1–expressing APCs. Video 1 shows FRAP of MHCII in a mature BMDC. Online supplemental material is available at http://www.jcb.org/cgi/content/full/jcb.201406120/DC1.

We thank members of the Burkhardt laboratory for helpful discussions and critical reading of the manuscript, Dr. Michael Edidin for helpful guidance, and Dr. Minsoo Kim for generously providing reagents. We thank the NAPCore and Flow Cytometry core facilities at the Children's Hospital of Philadelphia for time and assistance.

This work was supported by National Institutes of Health grants R01AI065644, P01CA093615, and GM104867.

The authors declare no competing financial interests.

Submitted: 26 June 2014
Accepted: 17 November 2014

Downloaded from http://rupress.org/jcb/article-pdf/208/4/457/1586664/jcb_201406120.pdf by guest on 08 February 2026

References

Al-Alwan, M.M., G. Rowden, T.D. Lee, and K.A. West. 2001. The dendritic cell cytoskeleton is critical for the formation of the immunological synapse. *J. Immunol.* 166:1452–1456. http://dx.doi.org/10.4049/jimmunol.166.3.1452

Al-Alwan, M.M., R.S. Liwski, S.M. Haeryfar, W.H. Baldridge, D.W. Hoskin, G. Rowden, and K.A. West. 2003. Cutting edge: dendritic cell actin cytoskeletal polarization during immunological synapse formation is highly antigen-dependent. *J. Immunol.* 171:4479–4483. http://dx.doi.org/10.4049/jimmunol.171.9.4479

Allenspach, E.J., P. Cullinan, J. Tong, Q. Tang, A.G. Tesciuba, J.L. Cannon, S.M. Takahashi, R. Morgan, J.K. Burkhardt, and A.I. Sperling. 2001. ERM-dependent movement of CD43 defines a novel protein complex distal to the immunological synapse. *Immunity*. 15:739–750. http://dx.doi.org/10.1016/S1074-7613(01)00224-2

Appel, H., L. Gauthier, J. Pyrdol, and K.W. Wucherpfennig. 2000. Kinetics of T-cell receptor binding by bivalent HLA-DR. Peptide complexes that activate antigen-specific human T-cells. *J. Biol. Chem.* 275:312–321. http://dx.doi.org/10.1074/jbc.275.1.312

Axelrod, D., D.E. Koppel, J. Schlessinger, E. Elson, and W.W. Webb. 1976. Mobility measurement by analysis of fluorescence photobleaching recovery kinetics. *Biophys. J.* 16:1055–1069. http://dx.doi.org/10.1016/S0006-3495(76)85755-4

Babich, A., S. Li, R.S. O'Connor, M.C. Milone, B.D. Freedman, and J.K. Burkhardt. 2012. F-actin polymerization and retrograde flow drive sustained PLCγ1 signaling during T cell activation. *J. Cell Biol.* 197:775–787. http://dx.doi.org/10.1083/jcb.201201018

Baker, R.G., C.J. Hsu, D. Lee, M.S. Jordan, J.S. Maltzman, D.A. Hammer, T. Baumgart, and G.A. Koretzky. 2009. The adapter protein SLP-76 mediates "outside-in" integrin signaling and function in T cells. *Mol. Cell. Biol.* 29:5578–5589. http://dx.doi.org/10.1128/MCB.00283-09

Barnden, M.J., J. Allison, W.R. Heath, and F.R. Carbone. 1998. Defective TCR expression in transgenic mice constructed using cDNA-based α- and β-chain genes under the control of heterologous regulatory elements. *Immunol. Cell Biol.* 76:34–40. http://dx.doi.org/10.1046/j.1440-1711.1998.00709.x

Barreiro, O., M. Yanez-Mo, J.M. Serrador, M.C. Montoya, M. Vicente-Manzanares, R. Tejedor, H. Furthmayr, and F. Sanchez-Madrid. 2002. Dynamic interaction of VCAM-1 and ICAM-1 with moesin and ezrin in a novel endothelial docking structure for adherent leukocytes. *J. Cell Biol.* 157:1233–1245. http://dx.doi.org/10.1083/jcb.200112126

Benvenuti, F., S. Hugues, M. Walmsley, S. Ruf, L. Fetler, M. Popoff, V.L. Tybulewicz, and S. Amigorena. 2004. Requirement of Rac1 and Rac2 expression by mature dendritic cells for T cell priming. *Science*. 305:1150–1153. http://dx.doi.org/10.1126/science.1099159

Billadeau, D.D., J.C. Nolz, and T.S. Gomez. 2007. Regulation of T-cell activation by the cytoskeleton. *Nat. Rev. Immunol.* 7:131–143. http://dx.doi.org/10.1038/nri2021

Boniface, J.J., J.D. Rabinowitz, C. Wülfing, J. Hampl, Z. Reich, J.D. Altman, R.M. Kantor, C. Beeson, H.M. McConnell, and M.M. Davis. 1998. Initiation of signal transduction through the T cell receptor requires the multivalent engagement of peptide/MHC ligands [corrected]. *Immunity*. 9:459–466. http://dx.doi.org/10.1016/S1074-7613(00)80629-9

Bouma, G., A. Mendoza-Naranjo, M.P. Blundell, E. de Falco, K.L. Parsley, S.O. Burns, and A.J. Thrasher. 2011. Cytoskeletal remodeling mediated by WASp in dendritic cells is necessary for normal immune synapse formation and T-cell priming. *Blood*. 118:2492–2501. http://dx.doi.org/10.1182/blood-2011-03-340265

Bretscher, A., K. Edwards, and R.G. Fehon. 2002. ERM proteins and merlin: integrators at the cell cortex. *Nat. Rev. Mol. Cell Biol.* 3:586–599. http://dx.doi.org/10.1038/nrm882

Brossard, C., V. Feuillet, A. Schmitt, C. Randriamampita, M. Romao, G. Raposo, and A. Trautmann. 2005. Multifocal structure of the T cell - dendritic cell synapse. *Eur. J. Immunol.* 35:1741–1753. http://dx.doi.org/10.1002/eji.200425857

Burkhardt, J.K., E. Carrizosa, and M.H. Shaffer. 2008. The actin cytoskeleton in T cell activation. *Annu. Rev. Immunol.* 26:233–259. http://dx.doi.org/10.1146/annurev.immunol.26.021607.090347

Cabañas, C., and N. Hogg. 1993. Ligand intercellular adhesion molecule 1 has a necessary role in activation of integrin lymphocyte function-associated molecule 1. *Proc. Natl. Acad. Sci. USA*. 90:5838–5842. http://dx.doi.org/10.1073/pnas.90.12.5838

Cairo, C.W., R. Mirchev, and D.E. Golan. 2006. Cytoskeletal regulation couples LFA-1 conformational changes to receptor lateral mobility and clustering. *Immunity*. 25:297–308. http://dx.doi.org/10.1016/j.immuni.2006.06.012

Carpén, O., P. Pallai, D.E. Staunton, and T.A. Springer. 1992. Association of intercellular adhesion molecule-1 (ICAM-1) with actin-containing cytoskeleton and α-actinin. *J. Cell Biol.* 118:1223–1234. http://dx.doi.org/10.1083/jcb.118.5.1223

Casares, S., C.S. Zong, D.L. Radu, A. Miller, C.A. Bona, and T.D. Brumeanu. 1999. Antigen-specific signaling by a soluble, dimeric peptide/major histocompatibility complex class II/Fc chimera leading to T helper cell type 2 differentiation. *J. Exp. Med.* 190:543–554. http://dx.doi.org/10.1084/jem.190.4.543

Celli, L., J.J. Ryckewaert, E. Delachanal, and A. Duperray. 2006. Evidence of a functional role for interaction between ICAM-1 and nonmuscle α-actinins in leukocyte diapedesis. *J. Immunol.* 177:4113–4121. http://dx.doi.org/10.4049/jimmunol.177.6.4113

Chen, W., and C. Zhu. 2013. Mechanical regulation of T-cell functions. *Immunol. Rev.* 256:160–176. http://dx.doi.org/10.1111/imr.12122

Chen, J., W. Yang, M. Kim, C.V. Carman, and T.A. Springer. 2006. Regulation of outside-in signaling and affinity by the β_2 I domain of integrin $\alpha_L\beta_2$. *Proc. Natl. Acad. Sci. USA*. 103:13062–13067. http://dx.doi.org/10.1073/pnas.0605666103

Chen, W., J. Lou, and C. Zhu. 2010a. Forcing switch from short- to intermediate- and long-lived states of the αA domain generates LFA-1/ICAM-1 catch bonds. *J. Biol. Chem.* 285:35967–35978. http://dx.doi.org/10.1074/jbc.M110.155770

Chen, X., C. Xie, N. Nishida, Z. Li, T. Walz, and T.A. Springer. 2010b. Requirement of open headpiece conformation for activation of leukocyte integrin $\alpha_X\beta_2$. *Proc. Natl. Acad. Sci. USA*. 107:14727–14732. http://dx.doi.org/10.1073/pnas.1008663107

Cochran, J.R., T.O. Cameron, and L.J. Stern. 2000. The relationship of MHC-peptide binding and T cell activation probed using chemically defined MHC class II oligomers. *Immunity*. 12:241–250. http://dx.doi.org/10.1016/S1074-7613(00)80177-6

Comrie, W., A. Babich, and J.K. Burkhardt. 2015. F-actin flow drives affinity maturation and spatial organization of LFA-1 at the immunological synapse. *J. Cell Biol.* 208:475–491.

Dehring, D.A., F. Clarke, B.G. Ricart, Y. Huang, T.S. Gomez, E.K. Williamson, D.A. Hammer, D.D. Billadeau, Y. Argon, and J.K. Burkhardt. 2011. Hematopoietic lineage cell-specific protein 1 functions in concert with the Wiskott-Aldrich syndrome protein to promote podosome array organization and chemotaxis in dendritic cells. *J. Immunol.* 186:4805–4818. http://dx.doi.org/10.4049/jimmunol.1003102

Delon, J., K. Kaibuchi, and R.N. Germain. 2001. Exclusion of CD43 from the immunological synapse is mediated by phosphorylation-regulated relocation of the cytoskeletal adaptor moesin. *Immunity*. 15:691–701. http://dx.doi.org/10.1016/S1074-7613(01)00231-X

Doty, R.T., and E.A. Clark. 1998. Two regions in the CD80 cytoplasmic tail regulate CD80 redistribution and T cell costimulation. *J. Immunol.* 161:2700–2707.

Dransfield, I., and N. Hogg. 1989. Regulated expression of Mg2+ binding epitope on leukocyte integrin alpha subunits. *EMBO J.* 8:3759–3765.

Dustin, M.L. 1998. Making a little affinity go a long way: a topological view of LFA-1 regulation. *Cell Adhes. Commun.* 6:255–262. http://dx.doi.org/10.3109/15419069809004481

Dustin, M.L., S.Y. Tseng, R. Varma, and G. Campi. 2006. T cell-dendritic cell immunological synapses. *Curr. Opin. Immunol.* 18:512–516. http://dx.doi.org/10.1016/j.coi.2006.05.017

Eun, S.Y., B.P. O'Connor, A.W. Wong, H.W. van Deventer, D.J. Taxman, W. Reed, P. Li, J.S. Blum, K.P. McKinnon, and J.P. Ting. 2006. Cutting edge: rho activation and actin polarization are dependent on plexin-A1 in dendritic cells. *J. Immunol.* 177:4271–4275. http://dx.doi.org/10.4049/jimmunol.177.7.4271

Feigelson, S.W., R. Pasvolsky, S. Cemerski, Z. Shulman, V. Grabovsky, T. Ilani, A. Sagiv, F. Lemaitre, C. Laudanna, A.S. Shaw, and R. Alon. 2010. Occupancy of lymphocyte LFA-1 by surface-immobilized ICAM-1 is critical for TCR- but not for chemokine-triggered LFA-1 conversion to an open headpiece high-affinity state. *J. Immunol.* 185:7394–7404. http://dx.doi.org/10.4049/jimmunol.1002246

Feng, C., Y.F. Li, Y.H. Yau, H.S. Lee, X.Y. Tang, Z.H. Xue, Y.C. Zhou, W.M. Lim, T.C. Cornvik, C. Ruedl, et al. 2012. Kindlin-3 mediates integrin αLβ2 outside-in signaling, and it interacts with scaffold protein receptor for activated-C kinase 1 (RACK1). *J. Biol. Chem.* 287:10714–10726. http://dx.doi.org/10.1074/jbc.M111.299594

Fisher, P.J., P.A. Bulur, S. Vuk-Pavlovic, F.G. Prendergast, and A.B. Dietz. 2008. Dendritic cell microvilli: a novel membrane structure associated with the multifocal synapse and T-cell clustering. *Blood*. 112:5037–5045. http://dx.doi.org/10.1182/blood-2008-04-149526

Gérard, A., O. Khan, P. Beemiller, E. Oswald, J. Hu, M. Matloubian, and M.F. Krummel. 2013. Secondary T cell-T cell synaptic interactions drive the differentiation of protective CD8+ T cells. *Nat. Immunol.* 14:356–363. http://dx.doi.org/10.1038/ni.2547

Girard, T., M. El-Far, D. Gaucher, O. Acuto, G. Beaulé, F. Michel, W. Mourad, and R.P. Sékaly. 2012. A conserved polylysine motif in

Downloaded from http://rupress.org/jcb/article-pdf/208/4/457/1586664/jcb_201406120.pdf by guest on 08 February 2026

CD86 cytoplasmic tail is necessary for cytoskeletal association and effective co-stimulation. *Biochem. Biophys. Res. Commun.* 423:301–307. http://dx.doi.org/10.1016/j.bbrc.2012.05.116

Grakoui, A., S.K. Bromley, C. Sumen, M.M. Davis, A.S. Shaw, P.M. Allen, and M.L. Dustin. 1999. The immunological synapse: a molecular machine controlling T cell activation. *Science*. 285:221–227. http://dx.doi.org/10.1126/science.285.5425.221

Gross, C.C., J.A. Brzostowski, D. Liu, and E.O. Long. 2010. Tethering of intercellular adhesion molecule on target cells is required for LFA-1-dependent NK cell adhesion and granule polarization. *J. Immunol.* 185:2918–2926. http://dx.doi.org/10.4049/jimmunol.1000761

Hamad, A.R., S.M. O'Herrin, M.S. Lebowitz, A. Srikrishnan, J. Bieler, J. Schneck, and D. Pardoll. 1998. Potent T cell activation with dimeric peptide-major histocompatibility complex class II ligand: the role of CD4 coreceptor. *J. Exp. Med.* 188:1633–1640. http://dx.doi.org/10.1084/jem.188.9.1633

Hogg, N., I. Patzak, and F. Willenbrock. 2011. The insider's guide to leukocyte integrin signalling and function. *Nat. Rev. Immunol.* 11:416–426. http://dx.doi.org/10.1038/nri2986

Huang, C., and T.A. Springer. 1997. Folding of the β-propeller domain of the integrin α_L subunit is independent of the I domain and dependent on the β2 subunit. *Proc. Natl. Acad. Sci. USA*. 94:3162–3167. http://dx.doi.org/10.1073/pnas.94.7.3162

Huppa, J.B., M. Axmann, M.A. Mörtelmaier, B.F. Lillemeier, E.W. Newell, M. Brameshuber, L.O. Klein, G.J. Schütz, and M.M. Davis. 2010. TCR-peptide-MHC interactions in situ show accelerated kinetics and increased affinity. *Nature*. 463:963–967. http://dx.doi.org/10.1038/nature08746

John, B., T.H. Harris, E.D. Tait, E.H. Wilson, B. Gregg, L.G. Ng, P. Mrass, D.S. Roos, F. Dzierszinski, W. Weninger, and C.A. Hunter. 2009. Dynamic Imaging of $CD8^+$ T cells and dendritic cells during infection with *Toxoplasma gondii*. *PLoS Pathog.* 5:e1000505. http://dx.doi.org/10.1371/journal.ppat.1000505

Judokusumo, E., E. Tabdanov, S. Kumari, M.L. Dustin, and L.C. Kam. 2012. Mechanosensing in T lymphocyte activation. *Biophys. J.* 102:L5–L7. http://dx.doi.org/10.1016/j.bpj.2011.12.011

Jun, C.D., M. Shimaoka, C.V. Carman, J. Takagi, and T.A. Springer. 2001. Dimerization and the effectiveness of ICAM-1 in mediating LFA-1-dependent adhesion. *Proc. Natl. Acad. Sci. USA*. 98:6830–6835. http://dx.doi.org/10.1073/pnas.121186998

Kim, M., C.V. Carman, and T.A. Springer. 2003. Bidirectional transmembrane signaling by cytoplasmic domain separation in integrins. *Science*. 301:1720–1725. http://dx.doi.org/10.1126/science.1084174

Kim, S.T., K. Takeuchi, Z.Y. Sun, M. Touma, C.E. Castro, A. Fahmy, M.J. Lang, G. Wagner, and E.L. Reinherz. 2009. The αβ T cell receptor is an anisotropic mechanosensor. *J. Biol. Chem.* 284:31028–31037. http://dx.doi.org/10.1074/jbc.M109.052712

Kim, S.T., Y. Shin, K. Brazin, R.J. Mallis, Z.Y. Sun, G. Wagner, M.J. Lang, and E.L. Reinherz. 2012. TCR mechanobiology: Torques and tunable structures linked to early T cell signaling. *Front. Immunol.* 3:76. http://dx.doi.org/10.3389/fimmu.2012.00076

Kinashi, T. 2005. Intracellular signalling controlling integrin activation in lymphocytes. *Nat. Rev. Immunol.* 5:546–559. http://dx.doi.org/10.1038/nri1646

Kong, F., A.J. García, A.P. Mould, M.J. Humphries, and C. Zhu. 2009. Demonstration of catch bonds between an integrin and its ligand. *J. Cell Biol.* 185:1275–1284. http://dx.doi.org/10.1083/jcb.200810002

Kong, F., Z. Li, W.M. Parks, D.W. Dumbauld, A.J. García, A.P. Mould, M.J. Humphries, and C. Zhu. 2013. Cyclic mechanical reinforcement of integrin-ligand interactions. *Mol. Cell*. 49:1060–1068. http://dx.doi.org/10.1016/j.molcel.2013.01.015

Lefort, C.T., Y.M. Hyun, J.B. Schultz, F.Y. Law, R.E. Waugh, P.A. Knauf, and M. Kim. 2009. Outside-in signal transmission by conformational changes in integrin Mac-1. *J. Immunol.* 183:6460–6468. http://dx.doi.org/10.4049/jimmunol.0900983

Levitsky, H.I., A. Lazenby, R.J. Hayashi, and D.M. Pardoll. 1994. In vivo priming of two distinct antitumor effector populations: the role of MHC class I expression. *J. Exp. Med.* 179:1215–1224. http://dx.doi.org/10.1084/jem.179.4.1215

Li, D., J.J. Molldrem, and Q. Ma. 2009. LFA-1 regulates $CD8^+$ T cell activation via T cell receptor-mediated and LFA-1-mediated Erk1/2 signal pathways. *J. Biol. Chem.* 284:21001–21010. http://dx.doi.org/10.1074/jbc.M109.002865

Li, Y.C., B.M. Chen, P.C. Wu, T.L. Cheng, L.S. Kao, M.H. Tao, A. Lieber, and S.R. Roffler. 2010. Cutting Edge: mechanical forces acting on T cells immobilized via the TCR complex can trigger TCR signaling. *J. Immunol.* 184:5959–5963. http://dx.doi.org/10.4049/jimmunol.0900775

Liu, G., A.T. Place, Z. Chen, V.M. Brovkovych, S.M. Vogel, W.A. Muller, R.A. Skidgel, A.B. Malik, and R.D. Minshall. 2012. ICAM-1-activated Src and eNOS signaling increase endothelial cell surface PECAM-1 adhesivity and neutrophil transmigration. *Blood*. 120:1942–1952. http://dx.doi.org/10.1182/blood-2011-12-397430

Liu, B., W. Chen, B.D. Evavold, and C. Zhu. 2014. Accumulation of dynamic catch bonds between TCR and agonist peptide-MHC triggers T cell signaling. *Cell*. 157:357–368. http://dx.doi.org/10.1016/j.cell.2014.02.053

Lu, C., M. Ferzly, J. Takagi, and T.A. Springer. 2001. Epitope mapping of antibodies to the C-terminal region of the integrin β 2 subunit reveals regions that become exposed upon receptor activation. *J. Immunol.* 166:5629–5637. http://dx.doi.org/10.4049/jimmunol.166.9.5629

Ma, Z., and T.H. Finkel. 2010. T cell receptor triggering by force. *Trends Immunol.* 31:1–6. http://dx.doi.org/10.1016/j.it.2009.09.008

Ma, Z., K.A. Sharp, P.A. Janmey, and T.H. Finkel. 2008. Surface-anchored monomeric agonist pMHCs alone trigger TCR with high sensitivity. *PLoS Biol.* 6:e43.

Miller, J., R. Knorr, M. Ferrone, R. Houdei, C.P. Carron, and M.L. Dustin. 1995. Intercellular adhesion molecule-1 dimerization and its consequences for adhesion mediated by lymphocyte function associated-1. *J. Exp. Med.* 182:1231–1241. http://dx.doi.org/10.1084/jem.182.5.1231

Monks, C.R., B.A. Freiberg, H. Kupfer, N. Sciaky, and A. Kupfer. 1998. Three-dimensional segregation of supramolecular activation clusters in T cells. *Nature*. 395:82–86. http://dx.doi.org/10.1038/25764

Nguyen, K., N.R. Sylvain, and S.C. Bunnell. 2008. T cell costimulation via the integrin VLA-4 inhibits the actin-dependent centralization of signaling microclusters containing the adaptor SLP-76. *Immunity*. 28:810–821. http://dx.doi.org/10.1016/j.immuni.2008.04.019

Ni, H.T., M.J. Deeths, and M.F. Mescher. 2001. LFA-1-mediated costimulation of $CD8^+$ T cell proliferation requires phosphatidylinositol 3-kinase activity. *J. Immunol.* 166:6523–6529. http://dx.doi.org/10.4049/jimmunol.166.11.6523

O'Connor, R.S., X. Hao, K. Shen, K. Bashour, T. Akimova, W.W. Hancock, L.C. Kam, and M.C. Milone. 2012. Substrate rigidity regulates human T cell activation and proliferation. *J. Immunol.* 189:1330–1339. http://dx.doi.org/10.4049/jimmunol.1102757

Oh, H.M., S. Lee, B.R. Na, H. Wee, S.H. Kim, S.C. Choi, K.M. Lee, and C.D. Jun. 2007. RKIKK motif in the intracellular domain is critical for spatial and dynamic organization of ICAM-1: functional implication for the leukocyte adhesion and transmigration. *Mol. Biol. Cell*. 18:2322–2335. http://dx.doi.org/10.1091/mbc.E06-08-0744

Oh, H.M., M.S. Kwon, H.J. Kim, B.H. Jeon, H.R. Kim, H.O. Choi, B.R. Na, S.H. Eom, N.W. Song, and C.D. Jun. 2011. Intermediate monomer-dimer equilibrium structure of native ICAM-1: implication for enhanced cell adhesion. *Exp. Cell Res.* 317:163–172. http://dx.doi.org/10.1016/j.yexcr.2010.10.004

Parameswaran, N., R. Suresh, V. Bal, S. Rath, and A. George. 2005. Lack of ICAM-1 on APCs during T cell priming leads to poor generation of central memory cells. *J. Immunol.* 175:2201–2211. http://dx.doi.org/10.4049/jimmunol.175.4.2201

Perez, O.D., D. Mitchell, G.C. Jager, S. South, C. Murriel, J. McBride, L.A. Herzenberg, S. Kinoshita, and G.P. Nolan. 2003. Leukocyte functional antigen 1 lowers T cell activation thresholds and signaling through cytohesin-1 and Jun-activating binding protein 1. *Nat. Immunol.* 4:1083–1092. http://dx.doi.org/10.1038/ni984

Reichardt, P., B. Dornbach, S. Rong, S. Beissert, F. Gueler, K. Loser, and M. Gunzer. 2007. Naive B cells generate regulatory T cells in the presence of a mature immunologic synapse. *Blood*. 110:1519–1529. http://dx.doi.org/10.1182/blood-2006-10-053793

Ross, R., H. Jonuleit, M. Bros, X.L. Ross, S. Yamashiro, F. Matsumura, A.H. Enk, J. Knop, and A.B. Reske-Kunz. 2000. Expression of the actin-bundling protein fascin in cultured human dendritic cells correlates with dendritic morphology and cell differentiation. *J. Invest. Dermatol.* 115:658–663. http://dx.doi.org/10.1046/j.1523-1747.2000.00112.x

Sabatos, C.A., J. Doh, S. Chakravarti, R.S. Friedman, P.G. Pandurangi, A.J. Tooley, and M.F. Krummel. 2008. A synaptic basis for paracrine interleukin-2 signaling during homotypic T cell interaction. *Immunity*. 29:238–248. http://dx.doi.org/10.1016/j.immuni.2008.05.017

Scholer, A., S. Hugues, A. Boissonnas, L. Fetler, and S. Amigorena. 2008. Intercellular adhesion molecule-1-dependent stable interactions between T cells and dendritic cells determine $CD8^+$ T cell memory. *Immunity*. 28:258–270. http://dx.doi.org/10.1016/j.immuni.2007.12.016

Schürpf, T., and T.A. Springer. 2011. Regulation of integrin affinity on cell surfaces. *EMBO J.* 30:4712–4727. http://dx.doi.org/10.1038/emboj.2011.333

Sprague, B.L., and J.G. McNally. 2005. FRAP analysis of binding: proper and fitting. *Trends Cell Biol.* 15:84–91. http://dx.doi.org/10.1016/j.tcb.2004.12.001

Springer, T.A., and M.L. Dustin. 2012. Integrin inside-out signaling and the immunological synapse. *Curr. Opin. Cell Biol.* 24:107–115. http://dx.doi.org/10.1016/j.ceb.2011.10.004

Downloaded from http://rupress.org/jcb/article-pdf/208/4/457/1586664/jcb_201406120.pdf by guest on 08 February 2026

Steenblock, E.R., T. Fadel, M. Labowsky, J.S. Pober, and T.M. Fahmy. 2011. An artificial antigen-presenting cell with paracrine delivery of IL-2 impacts the magnitude and direction of the T cell response. *J. Biol. Chem.* 286:34883–34892. http://dx.doi.org/10.1074/jbc.M111.276329

Tadokoro, S., S.J. Shattil, K. Eto, V. Tai, R.C. Liddington, J.M. de Pereda, M.H. Ginsberg, and D.A. Calderwood. 2003. Talin binding to integrin β tails: a final common step in integrin activation. *Science*. 302:103–106. http://dx.doi.org/10.1126/science.1086652

Thauland, T.J., and D.C. Parker. 2010. Diversity in immunological synapse structure. *Immunology*. 131:466–472. http://dx.doi.org/10.1111/j.1365-2567.2010.03366.x

Treanor, B., D. Depoil, A. Gonzalez-Granja, P. Barral, M. Weber, O. Dushek, A. Bruckbauer, and F.D. Batista. 2010. The membrane skeleton controls diffusion dynamics and signaling through the B cell receptor. *Immunity*. 32:187–199. http://dx.doi.org/10.1016/j.immuni.2009.12.005

Tseng, S.Y., M. Liu, and M.L. Dustin. 2005. CD80 cytoplasmic domain controls localization of CD28, CTLA-4, and protein kinase Cθ in the immunological synapse. *J. Immunol.* 175:7829–7836. http://dx.doi.org/10.4049/jimmunol.175.12.7829

Varga, G., N. Nippe, S. Balkow, T. Peters, M.K. Wild, S. Seeliger, S. Beissert, M. Krummen, J. Roth, C. Sunderkötter, and S. Grabbe. 2010. LFA-1 contributes to signal I of T-cell activation and to the production of T(h)1 cytokines. *J. Invest. Dermatol.* 130:1005–1012. http://dx.doi.org/10.1038/jid.2009.398

Verdijk, P., P.A. van Veelen, A.H. de Ru, P.J. Hensbergen, K. Mizuno, H.K. Koerten, F. Koning, C.P. Tensen, and A.M. Mommaas. 2004. Morphological changes during dendritic cell maturation correlate with cofilin activation and translocation to the cell membrane. *Eur. J. Immunol.* 34:156–164. http://dx.doi.org/10.1002/eji.200324241

Wang, Y., K. Shibuya, Y. Yamashita, J. Shirakawa, K. Shibata, H. Kai, T. Yokosuka, T. Saito, S. Honda, S. Tahara-Hanaoka, and A. Shibuya. 2008. LFA-1 decreases the antigen dose for T cell activation in vivo. *Int. Immunol.* 20:1119–1127. http://dx.doi.org/10.1093/intimm/dxn070

Wang, H., B. Wei, G. Bismuth, and C.E. Rudd. 2009. SLP-76-ADAP adaptor module regulates LFA-1 mediated costimulation and T cell motility. *Proc. Natl. Acad. Sci. USA*. 106:12436–12441. http://dx.doi.org/10.1073/pnas.0900510106

Xie, J., J.B. Huppa, E.W. Newell, J. Huang, P.J. Ebert, Q.J. Li, and M.M. Davis. 2012. Photocrosslinkable pMHC monomers stain T cells specifically and cause ligand-bound TCRs to be 'preferentially' transported to the cSMAC. *Nat. Immunol.* 13:674–680. http://dx.doi.org/10.1038/ni.2344

Xu, H., J.A. Gonzalo, Y. St Pierre, I.R. Williams, T.S. Kupper, R.S. Cotran, T.A. Springer, and J.C. Gutierrez-Ramos. 1994. Leukocytosis and resistance to septic shock in intercellular adhesion molecule 1-deficient mice. *J. Exp. Med.* 180:95–109. http://dx.doi.org/10.1084/jem.180.1.95

Yang, Y., C.D. Jun, J.H. Liu, R. Zhang, A. Joachimiak, T.A. Springer, and J.H. Wang. 2004. Structural basis for dimerization of ICAM-1 on the cell surface. *Mol. Cell*. 14:269–276. http://dx.doi.org/10.1016/S1097-2765(04)00204-7

Zhu, J., C.V. Carman, M. Kim, M. Shimaoka, T.A. Springer, and B.H. Luo. 2007. Requirement of α and β subunit transmembrane helix separation for integrin outside-in signaling. *Blood*. 110:2475–2483. http://dx.doi.org/10.1182/blood-2007-03-080077

Zhu, J., B.H. Luo, T. Xiao, C. Zhang, N. Nishida, and T.A. Springer. 2008. Structure of a complete integrin ectodomain in a physiologic resting state and activation and deactivation by applied forces. *Mol. Cell*. 32:849–861. http://dx.doi.org/10.1016/j.molcel.2008.11.018

Zhu, J., J. Zhu, and T.A. Springer. 2013. Complete integrin headpiece opening in eight steps. *J. Cell Biol.* 201:1053–1068. http://dx.doi.org/10.1083/jcb.201212037

Downloaded from http://rupress.org/jcb/article-pdf/208/4/457/1586664/jcb_201406120.pdf by guest on 08 February 2026